Learning-Enhanced Predictive Control and Experimental Validation of an Electro-Hydraulic Track Tensioning System for Tracked Vehicles

Zian Ding , Shufa Sun * , Hongxing Zhu , Zhiyong Yan , Yuan Zhou

Posted Date: 21 April 2026

doi: 10.20944/preprints202604.1445.v1

Keywords: electro-hydraulic tensioning system; learning enhancement; nonlinear model predictive control; adaptive weighting; co-simulation

 doi:10.20944/preprints202604.1445.v1

Article

Learning-Enhanced Predictive Control and Experimental Validation of an Electro-Hydraulic Track Tensioning System for Tracked Vehicles

Zian Ding [1], Shufa Sun [2,*], Hongxing Zhu [1], Zhiyong Yan [1] and Yuan Zhou [1]

[1] School of Mechanical and Electrical Engineering, Northeast Forestry University, Harbin, 15000, China

[2] School of Civil Engineering and Transportation, Northeast Forestry University, Harbin, 15000, China

* Correspondence: ad3301@163.com; Tel.: +8615504661751

Abstract

The electro-hydraulic track tensioning system of a tracked vehicle directly affects track engagement stability, vibration response, and energy utilization efficiency under complex terrain and time-varying loads. Accurate and robust control is therefore of great engineering significance. This paper focuses on an electro-hydraulic tensioning system with a composite actuation structure consisting of a proportional main valve and two 2/2 on-off valves, and proposes a learning-enhanced nonlinear model predictive control method (Learning-enhanced Nonlinear Model Predictive Control, L-NMPC). Residual learning, adaptive weight/constraint scheduling, and execution-layer mode coordination are integrated into a unified predictive control framework. The study is carried out on a strongly coupled Simulink–AMESim–RecurDyn co-simulation model and an LF1352 prototype-vehicle test platform. Comparative evaluations are conducted under steady step-and-ramp tracking, random rough terrain, sudden steering/braking pulses, supply-pressure limitation, and parameter drift/sudden-change conditions. The evaluation indices include track-tension tracking error, peak overshoot, settling time, energy consumption, and stability under parameter mismatch. Compared with conventional nonlinear model predictive control (NMPC), the proposed L-NMPC reduces the root-mean-square error of track tension by 42%–58%, decreases peak overshoot by 30%–40%, shortens settling time by 25%–35%, and achieves a 12%–17% reduction in energy consumption at the simulation level. Under ±20% parameter perturbation, the fluctuation of track tension can be constrained within ±1.1 kN. The simulation and real-vehicle results remain consistent in terms of the dominant dynamic trends and performance ranking. This study provides a verifiable implementation path for model–data-fusion control of strongly coupled electro-hydraulic actuation systems and offers an engineering reference for intelligent, energy-efficient, and highly reliable control of tracked-vehicle chassis systems.

Keywords: electro-hydraulic tensioning system; learning enhancement; nonlinear model predictive control; adaptive weighting; co-simulation

1. Introduction

Tracked vehicles are widely used in forestry operations, construction, and transportation over complex unstructured terrain because of their strong terrain adaptability and sustained traction capability. Under such operating conditions, the vehicle must maintain stable running and transmission boundaries in the presence of strong disturbances, time-varying loads, and limited hydraulic resources. Dynamic coordination and boundary control of the chassis system are therefore persistent research priorities [1]. Among the chassis subsystems, the electro-hydraulic tensioning system is one of the most sensitive boundary-control links under complex operating conditions because it simultaneously affects track engagement continuity, guide-wheel loading, vibration response, and energy utilization efficiency [2]. Compared with traditional mechanical or open-loop

 doi:10.20944/preprints202604.1445.v1

hydraulic tensioning devices, the electro-hydraulic tensioning system can realize dynamic regulation through closed-loop coordination of sensing, control, and actuation. It therefore offers greater freedom for track-tension optimization under complex conditions, while also introducing more pronounced nonlinearity, coupling, and constraints.

Research on track tensioning has already established a foundation in plant modeling, state estimation, and controller design. On the one hand, studies on the dynamic modeling of active tensioning systems, structural force-transmission mechanisms, and the relationship between control action and system response have clarified the evolution of track tension, guide-wheel behavior, and system dynamics, thus providing a basis for subsequent controller design. On the other hand, to improve sensing and online estimation of tension states, neural-network-based methods and related adaptive-control strategies have been explored, thereby enhancing observability and feedback capability at the tension boundary. At the system-validation level, Simulink–AMESim–RecurDyn multi-domain co-modeling has already been used to describe closed-loop coupling among the hydraulic, mechanical, and control domains, indicating that track-tension control has gradually moved from single-submodel analysis to cross-domain unified modeling and collaborative verification [3]. Meanwhile, studies on vibration tension control of high-speed track systems and on resistive-force simulation of hydraulic track-drive systems further show that track-tension problems are not limited to static preload settings, but are closely related to vehicle vibration characteristics, external resistance environments, and drive-system operating states [4,5].

However, analyzing only the tensioning subsystem itself is still insufficient to resolve control degradation under complex operating conditions. It is therefore necessary to examine the problem from the broader perspective of electro-hydraulic control. From this viewpoint, performance improvement of complex hydraulic actuation systems no longer depends solely on the actuator itself, but increasingly on supply-boundary management, valve-topology optimization, and coordinated control strategies. In recent years, research on electro-hydraulic control valves, independent metering technology, fault-tolerant control, position–pressure coordinated control under varying supply pressure, and mode-switching control has gradually formed a relatively systematic methodological spectrum, providing important references for flow regulation, mode organization, and constraint handling in multi-actuator hydraulic systems [6–10]. Furthermore, studies on robust identification of mobile hydraulic systems, reviews of control strategies for hydrostatic transmissions, digital hydraulic valves, and advanced modeling of electro-hydraulic control modules for intelligent chassis systems indicate that the dynamic performance of complex electro-hydraulic objects is jointly constrained by supply conditions, valve topology, and actuator structure, and controller design therefore needs to remain consistent with the implementation mode of the execution layer [11–14]. At the control-method level, learning-enhanced nonlinear model predictive control, constrained nonlinear model predictive control, neural-network feedforward compensation, and model predictive control for independent-metering valves have been applied to hydraulic cylinders, hydraulic excavators, and synchronized multi-hydraulic systems, demonstrating the potential of model–data fusion and constrained optimization in complex hydraulic systems [15–18]. Meanwhile, research on guaranteed-performance control of electro-hydraulic actuators, higher-order sliding-mode control, and deep-reinforcement-learning-enhanced control also indicates that, as object nonlinearity and operating-condition complexity increase, reliance on a fixed nominal model alone makes it difficult to balance tracking accuracy, control smoothness, and energy objectives simultaneously [19–21]. In parallel, the development of standardized coupling frameworks based on the Functional Mock-up Interface, real-time simulation control, electro-mechanical-hydraulic joint simulation tests, and real-time structural-dynamics estimation of hydraulically driven flexible systems has made it possible to conduct coordinated analysis and closed-loop evaluation of the control, hydraulic, and mechanical domains on a unified time scale, thereby offering a more traceable technical path for controller validation in strongly coupled electro-hydraulic systems [22–25].

Although these studies provide an important foundation for modeling, control, and validation of electro-hydraulic track tensioning systems, at least three mutually related problems remain for this

 doi:10.20944/preprints202604.1445.v1

particular object. First, traditional NMPC is usually built on a static nominal model and fixed weighting configuration. When the supply capability changes, hydraulic parameters drift, or the track–ground contact boundary changes, prediction mismatch, delayed constraint activation, and control-performance degradation are likely to occur. Second, although learning-enhanced predictive control has shown promise in complex hydraulic systems, there is still a lack of coordinated control-layer/execution-layer design consistent with real valve logic for composite actuation structures that combine continuous regulation by a proportional main valve and discrete switching by branch valves. This may cause a structural disconnect between optimizer outputs and actual execution actions. Third, validation based on a single model or a single platform often fails to capture the combined effects of hydraulic transients, track-boundary variation, and vehicle-dynamics feedback, thereby limiting assessment of control applicability under strongly coupled operating conditions. For this reason, NMPC is selected here as the direct baseline because it already provides explicit constraint handling and a relatively mature engineering implementation basis, making it possible to reveal more directly the gains introduced by the learning-enhancement mechanism within the same predictive-control framework.

To address these issues, this study focuses on the electro-hydraulic track tensioning system of tracked vehicles, constructs a control-oriented model around a proportional-main-valve/dual-2/2-on-off-valve composite circuit, and introduces a learning-enhanced nonlinear model predictive control (L-NMPC) framework in a Simulink–AMESim–RecurDyn co-simulation environment. The proposed method performs online model correction through residual learning, coordinates tensioning accuracy, actuation smoothness, and energy objectives through adaptive weight and constraint scheduling, and ensures engineering realizability of the control law at the real execution layer through feasible proportional-valve/branch-valve mapping and mode management. On this basis, co-simulation and real-vehicle evaluations are further conducted under typical scenarios such as steady tracking, random disturbances, supply-pressure limitation, and parameter drift, thereby establishing a unified path for modeling, control, and validation of strongly coupled electro-hydraulic track-tensioning objects.

2. System Structure and Modeling

To support subsequent controller design and co-simulation analysis, the object structure and the fundamentals of dynamic modeling of the electro-hydraulic track tensioning system are first described.

2.1. Electro-Hydraulic Track Tensioning System Structure

The core function of the electro-hydraulic track tensioning system of a tracked vehicle is to maintain continuous engagement and balanced loading among the track, guide wheel, and road-wheel system. As a key boundary variable of the system, track tension has a decisive influence on transmission efficiency, ground-contact stability, and vibration characteristics. Insufficient tension leads to track slackness, engagement disengagement, and even derailment; excessive tension causes excessive friction between the guide wheel and the track links as well as additional energy loss. Therefore, adaptive regulation of track tension under complex operating conditions characterized by non-stationary loads, supply-pressure fluctuations, and terrain disturbances is a key issue in tracked-vehicle dynamic control.

For this reason, traditional mechanical tensioning systems and open-loop hydraulic tensioning systems have gradually become inadequate for control under complex operating conditions. Conventional mechanical tensioning systems usually provide a fixed preload through torsion bars or lock nuts; their structure is simple but lacks adaptability. Although hydraulic tensioning systems can regulate track tension to a certain extent through oil pressure, most of them are still open-loop structures and cannot respond in real time to disturbances over complex terrain. With the development of electro-hydraulic control and embedded computing platforms, the electro-hydraulic tensioning system (EHTS) has become an important research direction. The system generally consists

 doi:10.20944/preprints202604.1445.v1

of a hydraulic actuation unit, sensing and estimation modules, and a control unit. The hydraulic subsystem includes a tensioning cylinder, one proportional main valve, and two 2/2 on-off valves. Three operating modes—pressurization, holding, and pressure release—are achieved through continuous main-valve regulation and branch-valve mode switching. The sensing module acquires cylinder displacement, chamber pressure, and track-tension signals in real time, while the control unit generates commands based on NMPC or L-NMPC. Compared with traditional mechanical tensioning, this composite-valve electro-hydraulic structure enables dynamic regulation of the tension state under closed-loop conditions and reduces additional energy losses caused by continuous throttling through branch-valve mode management. The system structure and hydraulic-circuit principle are shown in Figure 1.

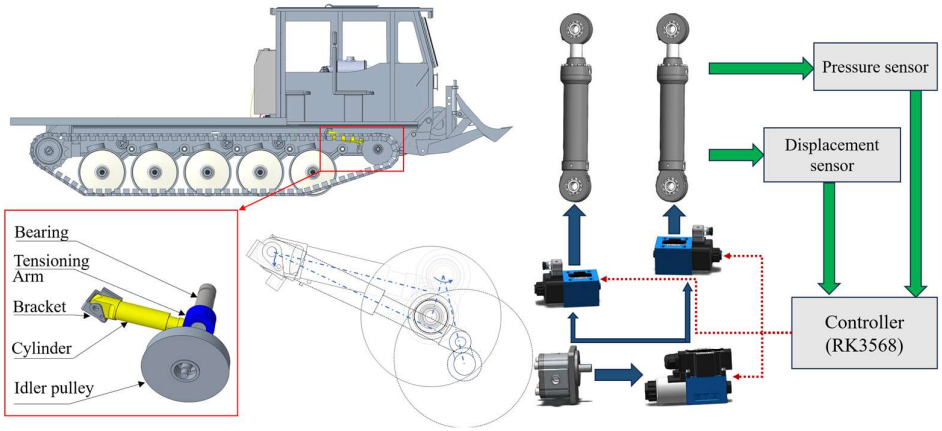

Figure 1. Hydraulic schematic of the tensioning system.

2.2. Hydraulic and Dynamic Modeling

To establish a control-oriented model of the tensioning system, it is first necessary to describe the basic relationships among valve-port flow, chamber pressure, and actuator motion. Figure 2 shows the equivalent hydraulic schematic of the electro-hydraulic track tensioning system. It abstracts the actual composite-valve circuit into a hydraulic network suitable for control analysis and provides a unified object representation for subsequent state-space modeling.

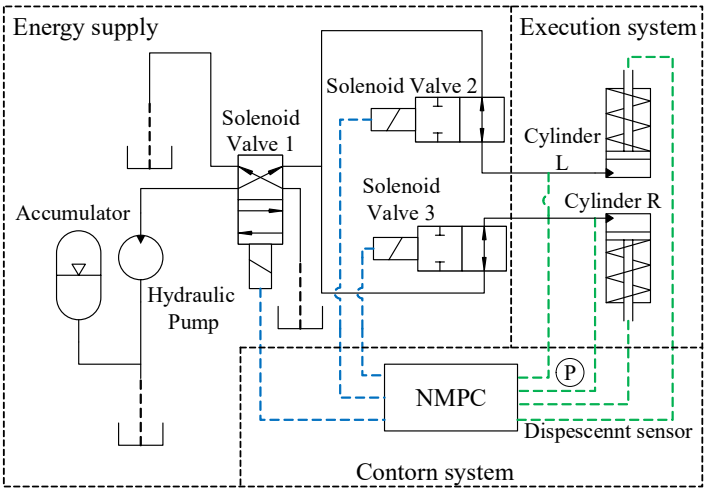

Figure 2. Equivalent hydraulic schematic of the system.

The dynamic process of the hydraulic actuation system is mainly described by the valve-port flow equation, chamber continuity equation, and actuator dynamic equation. The opening of the

 doi:10.20944/preprints202604.1445.v1

proportional main valve determines the effective flow area of the orifice, thereby affecting the flow input to the cylinder chambers; chamber-pressure variations are simultaneously affected by oil compressibility, effective volume variation, and leakage effects.

$$Q_v = C_q A_v(u)\sqrt{\left(\frac{2}{\rho}(p_S - p_L)\right)} \tag{1}$$

where C_q is the flow coefficient, A_v is the valve-opening function, ρ is the oil density, and p_S and p_L denote the supply and load pressures, respectively. Considering oil compressibility and leakage, the chamber-pressure dynamics satisfy:

$$\dot{p}_L = \frac{\beta_e}{V(y)}\left(Q_v - A_p\dot{y} - C_t p_L\right) \tag{2}$$

where β_e is the effective bulk modulus of the oil, V is the effective volume, A_p is the effective piston area, and C_t is the leakage coefficient. The output force of the tensioning cylinder is given by:

$$F_t = A_p p_L - F_f(\dot{y}) \tag{3}$$

where F_f is the friction force. These equations jointly describe the nonlinear coupling among valve-port flow, chamber-pressure variation, and piston motion, providing the dynamic basis for controller design. The tensioning cylinder is connected to the track boundary, and its motion can be described by Newton's second law as follows:

$$M_{cy}\ddot{y} = A_p(p_L - p_R) - F_{load}(t) \tag{4}$$

where M_{cy} is the equivalent moving mass and F_{load} is the external force generated by the track–ground interaction. Under loading, the track links can be approximately modeled as Euler–Bernoulli beams, whose deformation satisfies:

$$EI\frac{\theta^4 w(x,t)}{\theta x^4} + \rho A\frac{\theta^2 w(x,t)}{\theta t^2} = q(x,t) \tag{5}$$

where E is the elastic modulus of the links, I is the second moment of area of the cross-section, m is the mass per unit length, and q is the external load distribution. Under typical tracked-vehicle conditions, the tensioning system may exhibit markedly different load levels in steady and dynamically disturbed states; therefore, the control model needs to account for both steady-state maintenance and transient response capability.

2.3. State-Space Model and Control Objectives

By combining the hydraulic model with the mechanical-boundary dynamics, the tensioning system can be written in a control-oriented state-space form:

$$x = [p_L, p_R, y, \dot{y}]^T \tag{6}$$

where p_L and p_R are the left and right chamber pressures, y and $\dot{y}$ denote displacement and velocity, respectively, the control input is the valve opening, and the system output is the track tension. The nonlinear state equations can be written as:

$$\dot{x} = f(x,u), F_t = g(x,u) \tag{7}$$

In discrete form, one obtains:

$$x_{k+1} = f_d(x_k,u_k), F_t(k) = g_d(x_k,u_k) \tag{8}$$

The control objective is to minimize the tension-tracking error and control cost over a finite prediction horizon while satisfying physical constraints on pressure, actuator stroke, and valve opening. The tension-control problem can thus be formulated as a constrained nonlinear rolling optimization problem, which forms the basis for the subsequent NMPC design.

 doi:10.20944/preprints202604.1445.v1

2.4. Nonlinear Model Predictive Control (NMPC) Design

Nonlinear model predictive control (NMPC) performs rolling optimization of future input sequences over a finite prediction horizon based on the system model, thereby achieving constrained dynamic control.

$$J = \sum_{i=0}^{N_p} \left\| F_t(k+i|k) - F_{ref}(k+i|k) \right\|_Q^2 + \sum_{i=0}^{N_c-1} \|\Delta u(k+i|k)\|_R^2 \tag{9}$$

where Q and R are the weighting matrices for the tension-tracking error and control increment, respectively, and N_p and N_c denote the prediction and control horizons. The optimization problem is subject to the system dynamics and physical constraints:

$$x(k+i+1|k) = f_d\big(x(k+i|k), u(k+i|k)\big), u(k+i|k) \in U \tag{10}$$

where u_{min} and u_{max} denote the allowable valve-opening bounds, p_{min} and p_{max} denote the chamber-pressure limits, and y_{min} and y_{max} denote the actuator-stroke limits.

After optimization, only the first control action is applied, and prediction and optimization are repeated at the next sampling instant. This receding-horizon mechanism enables the controller to continuously obtain an optimal solution under non-stationary operating conditions. Because NMPC can explicitly handle pressure, valve-opening, and flow constraints while maintaining good control accuracy under nominal conditions, it has been widely used in complex electro-hydraulic systems. However, its performance depends strongly on model accuracy. When the hydraulic system is subjected to supply-pressure fluctuations, oil-temperature changes, or mechanical wear, the mismatch between the prediction model and the real system accumulates gradually, leading to increased overshoot, slower settling, and higher energy cost. To address this issue, a learning-enhancement mechanism is introduced into the NMPC framework, giving rise to the learning-enhanced nonlinear model predictive control (L-NMPC) method for online self-correction and adaptive tuning of control parameters.

2.5. Learning-Enhanced Nonlinear Model Predictive Control (L-NMPC)

L-NMPC introduces online learning and weight scheduling into the prediction–optimization structure of conventional NMPC in order to correct model bias and dynamically adjust the optimization objective. Through a data-driven incremental update mechanism, the algorithm maintains consistency between the model and the real system, thereby preserving stable control performance under complex operating conditions.

At the model level, L-NMPC uses recursive least squares (RLS) to estimate the linearized system parameters online and updates the prediction model using the latest measurements, thereby reducing model mismatch caused by supply-pressure variations and parameter disturbances. The corrected model maintains high consistency under changing supply conditions and parameter perturbations. To further capture the strong nonlinear characteristics of the hydraulic system—such as spool lag, fluid compressibility lag, and terrain-impact effects—a lightweight feedforward neural network (FNN) is introduced to learn the model residual. The network output is used as a correction term for the prediction error, endowing the model with self-learning capability and nonlinear compensation characteristics.

At the optimization level, L-NMPC introduces an adaptive weighting mechanism that dynamically adjusts the tracking-error weight Q and the energy weight R according to the system operating state. When the tension error or supply-pressure fluctuation increases, the controller automatically raises the accuracy weight to strengthen the response; when the system approaches a steady state, it reduces the energy weight to suppress throttling losses and valve chattering. Through this dynamic trade-off, the control law can achieve a better balance between accuracy and efficiency. The optimization problem of L-NMPC is written as:

 doi:10.20944/preprints202604.1445.v1

$$J_k^L = \sum_{i=0}^{N_p-1} \left\| F_{ten,k+i|k} - F_{ref,k+i} \right\|_{Q_k}^2 + \sum_{i=0}^{N_c-1} \left\| \Delta u_{k+i|k} \right\|_{R_k}^2 + \rho_k \|\varepsilon_k\|^2 \tag{11}$$

subject to

$$\begin{gathered} x_{k+i+1|k} = \hat{f}_k\left(x_{k+i|k}, u_{k+i|k}\right) + \hat{d}_k, u_{min} \le u_{k+i|k} \le u_{max} \\ p_{min} \le p_{k+i|k} \le p_{max}, y_{min} \le y_{k+i|k} \le y_{max}, \varepsilon_k \ge 0 \end{gathered} \tag{12}$$

where $\hat{f}_k(\cdot)$ denotes the prediction model updated online by the learning module, $\hat{d}_k$ is the residual correction term, Q_k and R_k are the adaptive weighting matrices scheduled according to the system state, ρ_k is the soft-constraint penalty factor, and ε_k is the slack variable introduced to maintain feasibility under constraint activation.

Compared with conventional NMPC, L-NMPC shows clear advantages in model consistency, optimization self-adjustment, and real-time implementability. Its online-learning mechanism suppresses the accumulation of model error through recursive estimation and residual compensation, so that the prediction model remains physically self-consistent in disturbed environments. Dynamic tuning of the cost function improves energy utilization without sacrificing stability and reduces high-frequency losses caused by frequent valve switching. By realizing coordinated updating of prediction, optimization, and learning within a unified control period, L-NMPC improves dynamic tracking accuracy and energy utilization of the tensioning system under complex operating conditions, and provides a unified control framework for the subsequent simulation and real-vehicle validation.

3. Three-Platform Co-Simulation and Comparison of Control Strategies

3.1. Control-Algorithm Application Architecture

To systematically evaluate the performance differences between different control strategies for the electro-hydraulic track tensioning system of tracked vehicles, a strongly coupled co-simulation framework is established on Simulink–AMESim–RecurDyn, where conventional nonlinear model predictive control (NMPC) and learning-enhanced nonlinear model predictive control (L-NMPC) are implemented under a unified object, unified boundaries, and unified scenario inputs. Simulink is responsible for controller solution, state estimation, and signal coordination; AMESim models the pressure–flow transients of the composite-valve hydraulic circuit; and RecurDyn calculates the multibody dynamic response of the track–guide wheel–vehicle body system. Data are exchanged at a unified time step, forming a consistent closed-loop coupling structure across the control, hydraulic, and mechanical domains. Figure 3 shows the overall architecture of the three-platform co-simulation and its cross-domain closed-loop data flow.

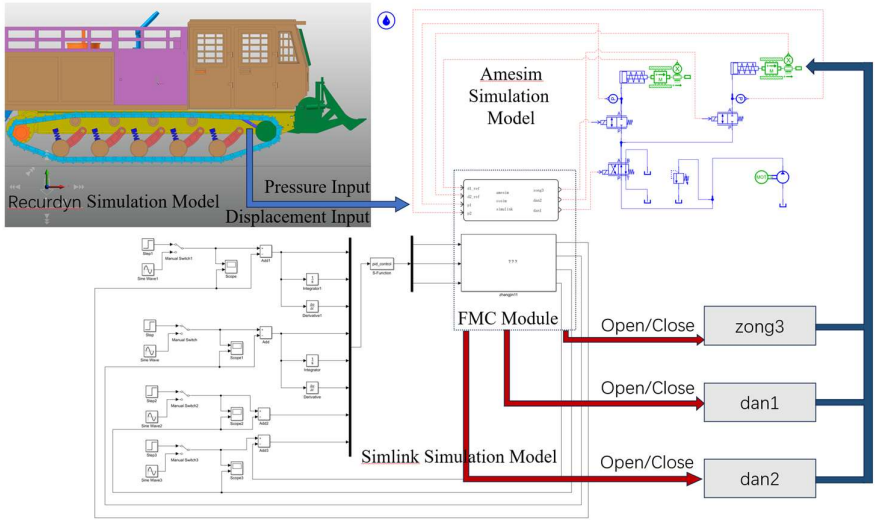

Figure 3. Co-simulation architecture.

 doi:10.20944/preprints202604.1445.v1

As shown in Figure 3, the controller generates valve commands according to the tension-force reference and the system feedback state. The hydraulic subsystem computes the chamber pressures and actuator displacement from the valve opening and supply condition. The multibody dynamic model further updates the contact load and system response according to guide-wheel displacement and track-boundary variation, and feeds the external load back to the controller and hydraulic model. The significance of this organization lies in the fact that co-simulation is no longer a simple concatenation of multiple software platforms, but a real dynamic loop established for control analysis under unified timing and boundary conditions. Compared with single-platform or locally equivalent modeling, this structure can simultaneously reflect the combined influence of hydraulic transients, actuator dynamics, and mechanical-boundary changes on tension-control performance, thereby providing a unified controlled object and unified boundary conditions for subsequent multi-scenario comparisons.

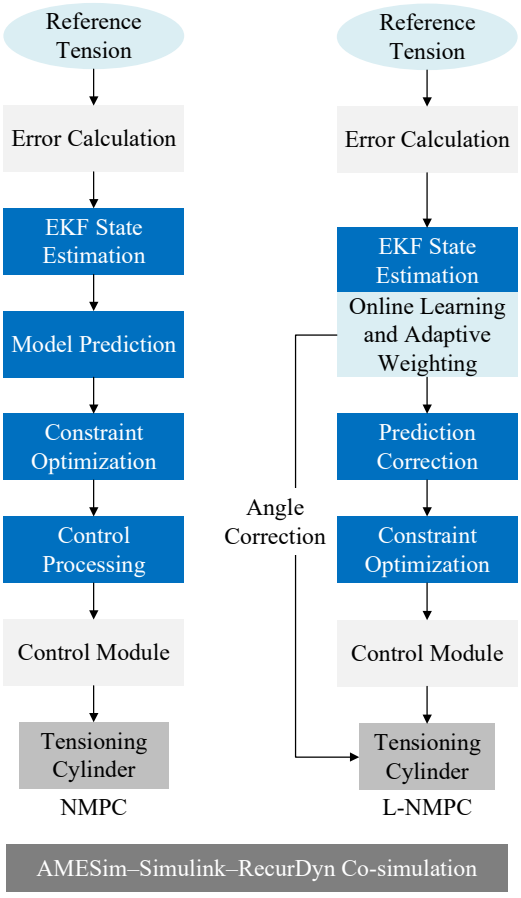

Figure 4. Architecture of NMPC and L-NMPC.

Figure 4 presents the control architecture of NMPC and L-NMPC for the electro-hydraulic tensioning system, where the latter further introduces learning correction and weight scheduling on top of the standard receding-horizon optimization framework. Using the tension-force error as the core feedback signal, the system acquires chamber-state variables in real time through pressure and displacement sensors. An extended Kalman filter (EKF) is then used for state reconstruction and noise suppression to obtain a more observable state vector. At each sampling instant, the estimation module provides the state vector required by the prediction model, including chamber pressures, piston displacement, and its rate, thus supplying consistent initial conditions for rolling optimization.

At the control level, L-NMPC still uses the receding-horizon optimization framework of NMPC as its basis, but further introduces online learning and adaptive weighting. The optimizer solves the future control sequence over a finite prediction horizon using the hydraulic and dynamic prediction

 doi:10.20944/preprints202604.1445.v1

models, and obtains the optimal valve-opening command by minimizing in real time a weighted quadratic cost on tension deviation and control increment. Meanwhile, the learning module constructs an empirical mapping of "state–input–response" from historical operating data and performs online fitting and correction of model residuals through recursive least squares or a lightweight neural network. The correction results are used to update the key linearization parameters and bias terms of the prediction model dynamically, enabling the model to maintain higher consistency under oil-temperature variation, valve lag, or friction changes.

At the energy-management and constraint layer, L-NMPC introduces an energy-aware weight-scheduling mechanism. According to the real-time energy curve, pressure fluctuation amplitude, and valve-opening variation rate, the controller automatically adjusts the weighting matrix in the cost function so as to achieve a dynamic balance between accuracy and efficiency. Under steady-state or light-load conditions, the input-penalty weight is reduced to decrease throttling losses; under supply-pressure drops or high-frequency disturbances, the constraint weight is raised to strengthen stability and robustness. Through this adaptive weighting mechanism, L-NMPC can dynamically balance tension accuracy, input smoothness, and energy cost under different operating conditions, thereby reducing ineffective regulation and additional throttling losses.

Because the system uses a composite-valve actuation structure, the optimizer output must be further mapped into implementable valve logic. Through the I/O mapping module, the control signal is converted into three-valve logic signals corresponding to the three operating modes of pressurize, hold, and release. Combined with minimum dwell-time constraints and dead-zone compensation, this logic makes the solenoid-valve actuation smoother and avoids hydraulic shocks caused by high-frequency switching. The hydraulic actuation unit, modeled in AMESim, acts on the tensioning cylinder and generates the corresponding tension-force feedback to the track–guide wheel–vehicle body system. RecurDyn computes the guide-wheel reaction and contact energy in real time and sends them back to the controller, thereby realizing bidirectional energy interaction among the hydraulic, control, and dynamic domains. The whole system uses a 1 ms master time step for FMI-based synchronous iteration, maintaining causality consistency in both time and energy.

To further verify the effectiveness of L-NMPC under complex operating conditions, the controller is embedded into the strongly coupled Simulink–AMESim–RecurDyn co-simulation framework, and five representative scenarios are constructed: steady-state step and ramp tracking, random rough terrain, sudden steering/braking pulses, supply-pressure limitation, and parameter drift/sudden change. These scenarios are used to systematically evaluate the overall performance gains of L-NMPC relative to conventional NMPC in terms of dynamic tracking, disturbance rejection, and energy utilization.

 doi:10.20944/preprints202604.1445.v1

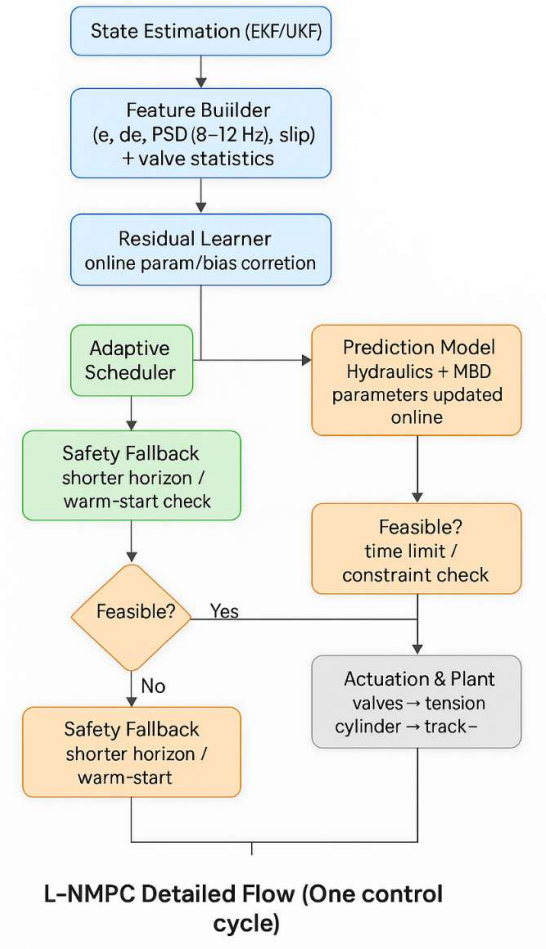

Figure 5. Logic diagram of L-NMPC.

To clarify the engineering meaning of the key weights, constraints, and scheduling parameters involved in Figure 5, Table 1 summarizes the main symbols used in the L-NMPC controller.

Table 1. Key symbols and engineering roles in the L-NMPC controller.

Symbol	Quantity (in L-NMPC)	Role in controller
Q_e	Weight on tension tracking error $e = F_{ten} - F_{ref}$	Accuracy vs. robustness trade-off
Q_{PSD}	Weight on vibration/PSD features (8–12 Hz band, body/guide-wheel accel.)	Penalizes resonance and high-frequency excitation
R_u	Weight on control increment Δu	Smoothness of valve commands, avoids chattering
ρ_{soft}	Penalty on slack variables (soft constraints)	How "hard" the pressure/force constraints are enforced
$P_{max,eff}$	Effective upper bound of chamber / supply pressure	Protects hydraulic components, shapes transient peaks
$T_{hold,min}$	Minimum on-time for each valve state (press/hold/release)	Limits valve switching frequency, reduces throttling loss
N_p	Prediction horizon (steps)	Look-ahead capability vs. real-time burden
$wenergy$	Weight on energy-related terms (throttling loss, valve activity)	Explicit energy–tracking trade-off

 doi:10.20944/preprints202604.1445.v1

3.2. Multi-Scenario Simulation

After the L-NMPC controller is established, it is embedded together with conventional NMPC into the strongly coupled Simulink–AMESim–RecurDyn co-simulation framework. Five representative scenarios are considered: steady-state step and ramp tracking (S1), random rough terrain (S2), sudden steering/braking pulses (S3), supply-pressure limitation (S4), and parameter drift/sudden change (S5). These scenarios correspond to typical operating states of the tensioning system under reference switching, broadband random disturbance, transient impact, shrinking supply boundary, and model mismatch, respectively, and together cover the main test conditions from nominal tracking to complex boundary constraints. Within this framework, the track–ground contact force and body vibration generated by RecurDyn are fed back to the AMESim hydraulic model in real time and, together with the controller, form a complete dynamically consistent loop. By collecting the tension response, control input, and cumulative energy under the five scenarios, the comprehensive advantages of L-NMPC in dynamic tracking, energy utilization, disturbance rejection, and model-mismatch conditions can be evaluated, thereby laying the foundation for subsequent real-vehicle validation.

For all scenarios, the NMPC and L-NMPC controllers in Simulink share the same horizons and constraint settings. AMESim provides detailed modeling of the hydraulic cylinder, valve throttling, fluid compliance, and supply dynamics, whereas RecurDyn provides the contact force, attitude variation, and vibration feedback of the track–guide wheel–vehicle body system, feeding them back to the controller and learning module in real time. This structure ensures that each control update is based on actual dynamic evolution rather than on equivalent force sources or frozen boundaries often used in traditional dual-platform simulations. The learning-enhancement mechanism of L-NMPC is activated explicitly in all five scenarios, so that adaptive response patterns different from those of conventional NMPC emerge when system load changes rapidly, excitation bands shift, supply pressure becomes limited, or parameters drift. The outputs collected from simulation include tension response, control input, key pressure states, and cumulative energy, which are then used for subsequent performance comparison and mechanism analysis. For convenience, Table 2 summarizes the core settings and evaluation focuses of the five simulation scenarios.

Table 2. Scenario settings and evaluation focuses for the five simulation cases.

Scenario ID	Scenario	Core setting	Evaluation focus
S1	Steady-state step and ramp tracking	Reference tension steps from 12 kN to 15 kN and a gradual ramp input is superimposed	Tracking accuracy, settling time, energy variation
S2	Random rough terrain	Broadband random disturbance is introduced under a constant tension target	Disturbance rejection, fluctuation suppression, energy growth
S3	Sudden steering/braking pulses	Positive and negative pulse loads are applied on top of steady tensioning	Peak suppression, recovery capability, input smoothness
S4	Supply-pressure limitation	The supply boundary decreases and then recovers	Feasibility maintenance, boundary coordination, energy cost
S5	Parameter drift and sudden change	Staged parameter drift and mismatch are introduced	Robustness, online adaptability, steady-state retention

Based on the above scenario definitions, the response characteristics of NMPC and L-NMPC are compared in detail under each representative operating condition.

 doi:10.20944/preprints202604.1445.v1

3.2.1. Steady-State Step and Ramp Tracking

The steady-state step-and-ramp tracking scenario is used to characterize the basic tracking performance of the tensioning system under the combined action of abrupt reference change and slowly varying target evolution. The main concerns are transient build-up capability, steady-state tracking accuracy, control-input smoothness, and cumulative energy variation. In this study, the reference tension is set to step from 12 kN to 15 kN at t = 3 s, and a gradual ramp drift of 0.05 kN/s is superimposed after t = 10 s so as to highlight the differences in controller response during the transient build-up and slow-varying tracking stages.

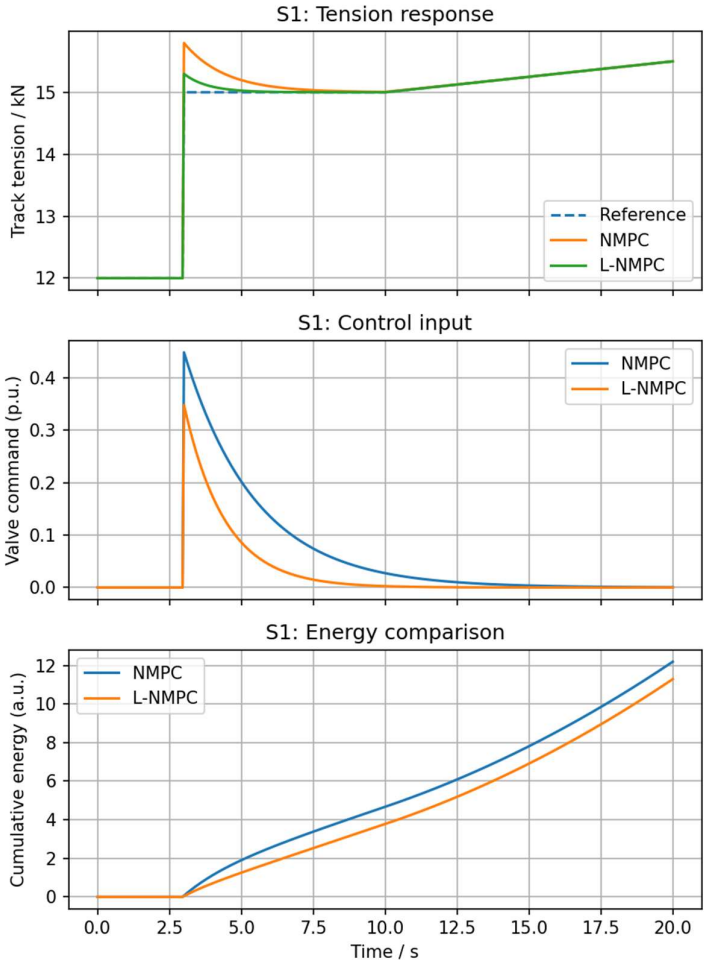

Figure 6. Comparison under the steady-state step-and-ramp scenario: (a) S1: tension response; (b) S1: control input; (c) S1: energy comparison.

Figure 6a compares the tension responses of the two control strategies. Both controllers can track the reference, but their dynamic qualities differ markedly. After the step switch, the peak value under NMPC is about 15.75–15.80 kN, corresponding to an overshoot of about 0.75–0.80 kN, whereas the peak value under L-NMPC is about 15.25–15.30 kN, corresponding to an overshoot of about 0.25–0.30 kN. The overshoot magnitude is therefore reduced by about 62%–67%. Meanwhile, L-NMPC settles much faster after the step and returns to the vicinity of 15 kN within about 2 s, whereas NMPC requires about 4–5 s to basically enter the steady region. During the ramp stage after 10 s, both algorithms can follow the slowly increasing target, but the L-NMPC curve is smoother overall and adheres more closely to the reference, indicating that it maintains better prediction consistency and steady-state tracking performance under slowly varying targets.

 doi:10.20944/preprints202604.1445.v1

Figure 6b compares the control inputs of the proportional main valve. The peak input of NMPC is about 0.45, whereas that of L-NMPC is about 0.35, a reduction of about 22%. At the same time, the input under L-NMPC decays faster and drops close to zero by about 7–8 s, while NMPC still exhibits a visible adjustment tail up to about 12–15 s. This indicates that L-NMPC does not achieve better tracking by relying on more aggressive valve action; instead, it establishes the target tension with a lower input amplitude and shorter actuation duration, thereby avoiding excessive local throttling losses and unnecessary fast regulation.

Figure 6c compares cumulative energy. At t = 20 s, the cumulative energy under NMPC is about 12.1 kJ, whereas that under L-NMPC is about 11.2 kJ, corresponding to an energy reduction of about 0.9 kJ or 7.4%. Although external disturbance and supply variation are not severe in this scenario, the learning-enhancement mechanism still exhibits better energy-utilization performance. This indicates that L-NMPC reduces the propagation of prediction bias through online correction and suppresses unnecessary repeated compensation through adaptive weighting, making the control input smoother while maintaining tracking capability and thereby reducing the growth rate of cumulative energy.

3.2.2. Random Rough Terrain Scenario

To characterize the disturbance-rejection performance of the tensioning system under broadband random excitation, a random-load excitation formed by superimposing multi-frequency sine components and Gaussian white noise is introduced in simulation. The reference tension is kept constant at 15 kN, and the random disturbance is fed back to the guide-wheel boundary through the track–ground contact model, thereby driving sustained fluctuations in the tensioning system. This scenario is mainly used to assess the controller's disturbance-rejection capability and vibration-suppression performance under complex non-stationary inputs.

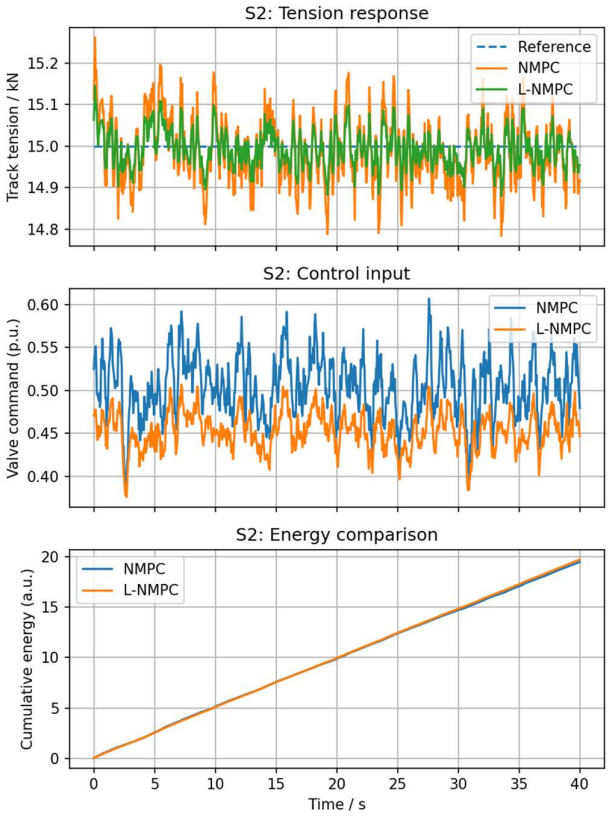

Figure 7. Comparison under the random rough terrain scenario: (a) S2: tension response; (b) S2: control input; (c) S2: energy comparison.

 doi:10.20944/preprints202604.1445.v1

Figure 7a presents the tension response under the random rough terrain scenario. Both controllers maintain the tension around 15 kN, but the dynamic quality differs significantly under sustained random excitation. The tension under NMPC fluctuates in the range of about 14.78–15.27 kN, with a peak-to-peak fluctuation of about 0.49 kN; under L-NMPC, the fluctuation range narrows to about 14.88–15.15 kN, with a peak-to-peak amplitude of about 0.27 kN, corresponding to a reduction of about 45%. Locally, NMPC still exhibits a considerable number of high-amplitude spikes after 20 s, whereas the fluctuations under L-NMPC are concentrated more tightly around the reference value. This indicates that the learning-enhancement mechanism can more effectively suppress the transmission of high-frequency disturbances to the tensioning loop under random rough terrain.

Figure 7b compares the control input of the proportional main valve. Under NMPC, the input is approximately distributed in the interval 0.45–0.61, with an average level of about 0.52; under L-NMPC, it is mainly distributed in the interval 0.39–0.50, with an average level of about 0.45, corresponding to a reduction of about 13%–15% in the mean input level. At the same time, the input under NMPC fluctuates more frequently and contains more spikes, whereas the input curve under L-NMPC is smoother overall. This suggests that under broadband random disturbance, L-NMPC does not suppress tension fluctuations by increasing actuator effort, but instead achieves better disturbance attenuation at a lower input level, thereby reducing unnecessary rapid valve regulation.

Figure 7c shows that the cumulative energy growth rate of L-NMPC remains lower than that of NMPC throughout the process, indicating that under random disturbance it not only yields a smaller tension-fluctuation envelope but also effectively suppresses the energy growth caused by frequent compensation and high-amplitude valve action. Overall, under sustained random excitation, L-NMPC exhibits better overall performance in fluctuation suppression, input smoothness, and energy utilization.

3.2.3. Sudden Steering/Braking Pulse Scenario

In this scenario, a +2 kN tension pulse is applied during t = 6–8 s and a −1.5 kN release pulse is applied during t = 18–20 s to simulate the rapid transition of guide-wheel boundary loads during sudden steering and emergency braking. The main concerns are the controller's capability for suppressing peak amplification, its recovery behavior, and its energy-utilization characteristics under abrupt external loads.

 doi:10.20944/preprints202604.1445.v1

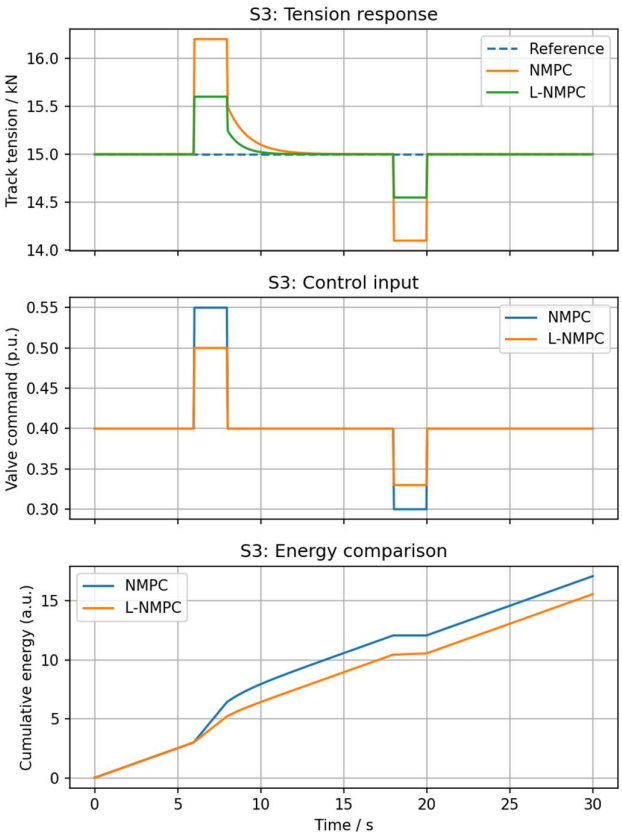

Figure 8. Comparison under the sudden steering/braking pulse scenario: (a) S3: tension response; (b) S3: control input; (c) S3: energy comparison.

Figure 8a shows that both controllers can keep the tension fluctuating around the reference under positive and negative pulses, but the dynamic quality differs clearly. During the positive pulse, the peak value under NMPC is about 16.2 kN, i.e., about 1.2 kN above the 15 kN baseline, whereas the peak under L-NMPC is about 15.6 kN, i.e., an increment of about 0.6 kN, corresponding to a reduction of about 50% in the peak increment. During the negative pulse, the minimum value under NMPC is about 14.10 kN, i.e., about 0.90 kN below the steady-state level, whereas the minimum under L-NMPC is about 14.55 kN, i.e., a drop of about 0.45 kN, again corresponding to about a 50% reduction in the negative deviation. In addition, after the end of the pulses, the tension curve of L-NMPC returns to the reference more quickly and exhibits a smoother transition, whereas NMPC shows a more obvious positive tail after the positive pulse and a deeper transient dip after the negative pulse. This indicates that the learning-enhancement mechanism can more effectively suppress the amplification of deviations induced by pulse-like impacts and improve the recovery process after the pulses.

Figure 8b shows the control-input variation. Compared with NMPC, L-NMPC exhibits smoother input changes during both positive and negative pulses and shows no pronounced high-amplitude spikes, indicating that it can reconstruct the control input more stably under transient impacts while avoiding excessive local compensation behavior.

Figure 8c compares cumulative energy. At t = 30 s, the cumulative energy under NMPC is about 17.1, whereas that under L-NMPC is about 15.5, corresponding to a difference of about 1.6 or a reduction of about 9.4%. At the first energy inflection after the positive pulse, the cumulative energy is about 6.6 under NMPC and about 5.3 under L-NMPC; near the second inflection after the negative pulse, the values are about 12.0 and 10.5, respectively. These results indicate that the learning-enhancement mechanism not only improves the time-domain tension response under pulse loads,

 doi:10.20944/preprints202604.1445.v1

but also reduces the growth rate of cumulative energy under abrupt loads by decreasing excessive compensation and repeated regulation.

3.2.4. Supply-Pressure-Limited Scenario

The supply-pressure-limited scenario is used to characterize the feasibility-maintenance and boundary-coordination capability of the tensioning system under a shrinking hydraulic supply boundary. The supply pressure is set to decrease gradually from 18 MPa to 12 MPa and then recover, thereby creating a supply-constrained interval under otherwise steady tensioning so as to highlight the dynamic-response differences of the control strategies during boundary changes. The main concerns are the drop amplitude of track tension, the transient peak during pressure switching, the smoothness of the recovery process, and the cumulative-energy growth behavior.

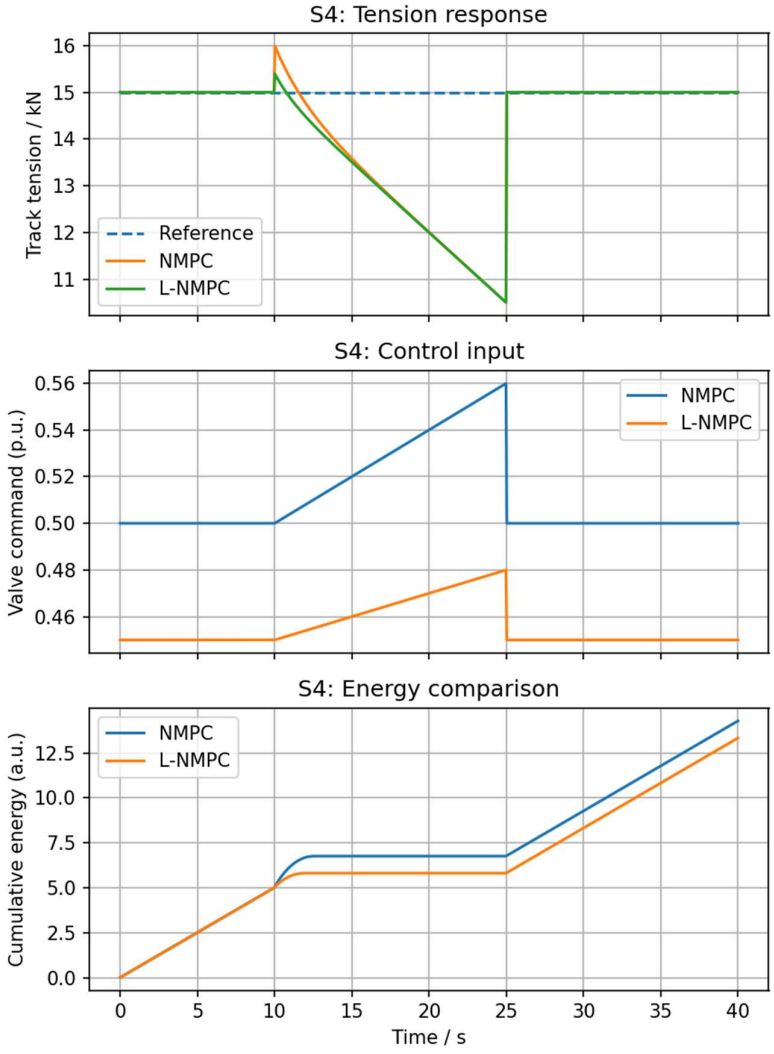

Figure 9. Comparison under the supply-pressure-limited scenario: (a) S4: tension response; (b) S4: control input; (c) S4: energy comparison.

Figure 9a shows that both controllers can bring the tension back to the reference vicinity after the supply pressure recovers, but their dynamic qualities still differ significantly during the instant of boundary switching and during the limited-supply stage. When the supply-limited stage begins, the instantaneous tension peak under NMPC is about 16.0 kN, i.e., about 1.0 kN above the 15 kN

 doi:10.20944/preprints202604.1445.v1

baseline, whereas the peak under L-NMPC is about 15.4 kN, corresponding to an increment of about 0.4 kN. The switching-induced peak increment is thus reduced by about 60%. This indicates that L-NMPC can more effectively suppress the transient peak amplification caused by control redistribution when the boundary changes abruptly. Subsequently, during the supply-limited interval, the tension under both algorithms decays continuously as the available supply pressure drops and finally decreases to about 10.5 kN. This indicates that under strong supply constraints, the ultimate tension-retention level is mainly dominated by the external supply boundary, and the controller has only limited influence on the final minimum level. Nevertheless, over the entire limited-supply interval, the early-stage transition under L-NMPC is smoother, indicating better constraint coordination during boundary switching.

Figure 9b shows that the control-input reconstruction of NMPC is much more drastic during the supply-limited stage, whereas the input change under L-NMPC is smoother and does not exhibit obvious abnormal spikes. It can therefore be seen that under a shrinking supply boundary, the learning-enhancement mechanism effectively mitigates input mutation caused by constraint switching and control redistribution.

Figure 9c shows that the cumulative-energy growth rate of L-NMPC is always lower than that of NMPC, and this scenario is also the one with the most pronounced energy improvement among all scenarios. This indicates that under limited supply, L-NMPC can not only suppress abnormal peak amplification during boundary switching, but also reduce additional energy costs caused by overcompensation and repeated adjustment through smoother control reconstruction.

3.2.5. Parameter Drift and Sudden-Change Scenario

To account for changes in hydraulic and mechanical parameters during long-term operation, the effective bulk modulus of the hydraulic oil, the equivalent friction coefficient of the cylinder, and the equivalent track stiffness are assigned staged cumulative drifts to represent combined mismatch effects such as increased oil compressibility, friction-state variation, and softening of the track loop. This scenario is used to verify the controller's adaptability and stability under parameter disturbances as well as the fault-tolerance of predictive control under model mismatch.

 doi:10.20944/preprints202604.1445.v1

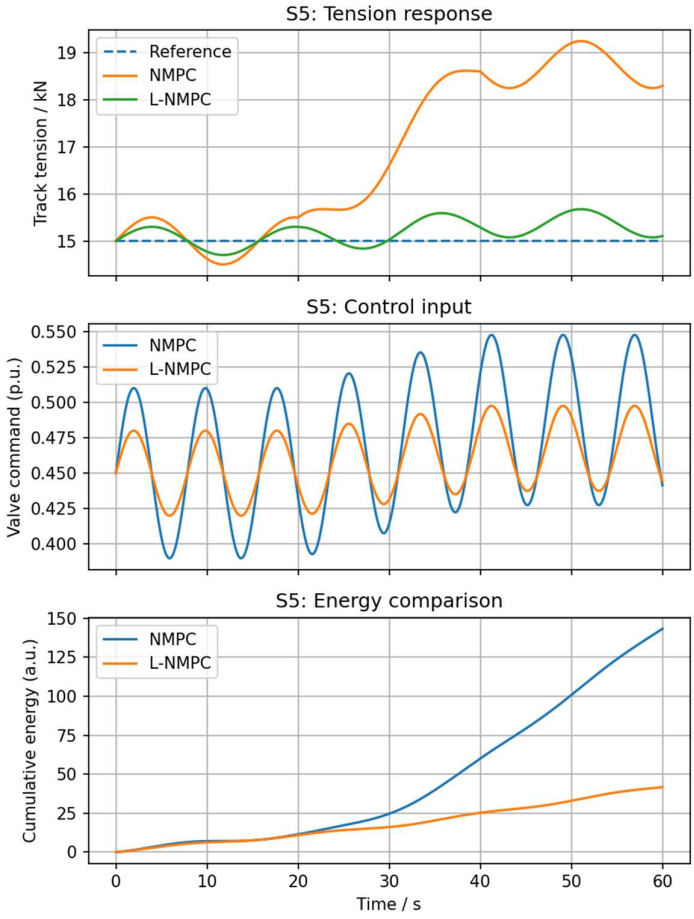

Figure 10. Comparison under the structural–hydraulic parameter-drift scenario: (a) S5: tension response; (b) S5: control input; (c) S5: energy comparison.

Figure 10a shows that under progressively accumulated parameter drift, the difference between the two controllers grows continuously over time. In the initial stage, NMPC is still able to keep the tension fluctuating slightly around the reference. However, from about 20 s onward, a clear steady-state offset appears, with the tension level continuing to rise and eventually stabilizing in the range of 18.3–19.2 kN, corresponding to a positive deviation of about 3.3–4.2 kN relative to the 15 kN reference. By contrast, L-NMPC remains within about 14.8–15.7 kN, with the steady-state offset controlled within about ±0.7 kN. It follows that under staged cumulative parameter drift, NMPC is much more sensitive to nominal-model mismatch: as the drift intensifies, prediction errors accumulate and ultimately manifest as a pronounced tension bias. In contrast, L-NMPC effectively suppresses the expansion of this bias through online correction and weight scheduling, keeping the tension response close to the reference throughout the process.

Figure 10b compares the control input of the proportional main valve. Under NMPC, the input is approximately distributed in the interval 0.39–0.55, with a peak-to-peak variation of about 0.16; under L-NMPC, it is mainly distributed in 0.42–0.50, with a variation amplitude of about 0.08, i.e., about 50% smaller than that of NMPC. Moreover, as the degree of parameter drift increases, the input amplitude under NMPC tends to increase progressively, whereas the input variation under L-NMPC remains within a much narrower range. This indicates that under long-term model mismatch, L-NMPC does not compensate for drift through more aggressive actuation, but rather stabilizes the tension boundary at a lower level of input fluctuation, thereby suppressing unnecessary rapid regulation and overcompensation.

 doi:10.20944/preprints202604.1445.v1

Figure 10c shows that the cumulative energy under L-NMPC remains lower than that under NMPC throughout the drift process, and that the energy-growth rate is more stable. Overall, under parameter drift, L-NMPC can confine the fluctuation of track tension to a relatively small range, whereas conventional NMPC exhibits evident steady-state bias and amplified oscillation once mismatch accumulates. This indicates that the learning-enhancement mechanism has stronger adaptability and robustness under long-term model mismatch.

3.3. Discussion

Based on the Simulink–AMESim–RecurDyn three-platform co-simulation environment, this section systematically compares the control performance of NMPC and L-NMPC for the electro-hydraulic tensioning system under five representative scenarios: steady-state step and ramp tracking, random rough terrain, sudden steering/braking pulses, supply-pressure limitation, and parameter drift/sudden change. The simulation results show that both controllers can accomplish tension regulation under all scenarios, but they exhibit markedly different dynamic characteristics in the presence of complex disturbances, changing supply boundaries, and model mismatch.

Overall, conventional NMPC can achieve acceptable basic tracking under nominal conditions, but its performance strongly depends on model accuracy and fixed weighting configuration. When external disturbances intensify, the supply boundary changes, or system parameters continue to drift, NMPC is more likely to exhibit excessive peak response, prolonged recovery, intensified input oscillation, and accelerated cumulative-energy growth. This indicates that under strongly coupled and time-varying boundary conditions, reliance solely on a static nominal model and fixed optimization structure makes it difficult to maintain the dynamic consistency and constraint-coordination capability of the tensioning system over the long term.

In contrast, L-NMPC exhibits more stable control quality across all five scenarios. Under steady-state step and ramp tracking, the learning-enhancement mechanism effectively suppresses overshoot and improves recovery; under random rough terrain and sudden steering/braking pulses, both the fluctuation amplitude of track tension and the transient peaks are significantly reduced, indicating better suppression of broadband disturbances and abrupt external loads; under supply-pressure limitation, L-NMPC attenuates abnormal peak amplification caused by supply-boundary switching while maintaining smoother input reconstruction; under parameter drift and sudden change, L-NMPC shows stronger adaptability to long-term model mismatch and can maintain stable tension within a smaller input fluctuation range, thereby avoiding obvious steady-state bias and oscillation amplification.

Mechanistically, the performance improvement of L-NMPC mainly arises from three aspects. First, the online-learning mechanism reduces the prediction bias between the nominal model and the real object, enabling the rolling optimization to be carried out on a model closer to the actual system dynamics. Second, adaptive weight and constraint scheduling improves the dynamic balance among tension accuracy, input smoothness, and energy objectives under different operating conditions, allowing the controller to shift its optimization emphasis according to the running state. Third, the coordinated execution-layer mode management of the proportional main valve and the two on-off valves ensures that the optimization result can be stably mapped into physically implementable valve actions, thereby improving the engineering realizability of the control strategy under a composite actuation structure.

These results indicate that, compared with conventional NMPC, L-NMPC provides better cross-scenario adaptability, higher dynamic stability, and superior energy utilization in the electro-hydraulic track tensioning system of tracked vehicles. They provide a simulation basis for subsequent real-vehicle validation and a foundation for control-strategy design of electro-hydraulic tensioning systems under complex operating conditions. It should be noted that the conclusions in this section are mainly based on three-platform co-simulation results, and the controller's generalization capability under longer time horizons, on more vehicle types, and under more complex supply boundaries still needs to be further evaluated in combination with subsequent experiments.

 doi:10.20944/preprints202604.1445.v1

4. Experimental Validation

After completing the co-simulation assessment, it is necessary to further verify the adaptability and engineering implementability of the control strategy in a real hydraulic–mechanical coupled environment. Accordingly, experimental validation is carried out.

4.1. Test Platform Construction

To verify the control performance of NMPC and L-NMPC in a real hydraulic–mechanical coupled environment, an electro-hydraulic track tensioning test platform is built on the LF1352 tracked vehicle. Two custom hydraulic tensioning cylinders are arranged on both sides of the guide wheel, and a three-valve logic control circuit is configured. The circuit includes one Huade HD-4WREE6 four-way, three-position proportional directional valve and two normally closed two-position, two-way solenoid valves. This circuit can realize three operating modes—pressurization, holding, and release. The main supply pressure is provided by a gear pump, and an accumulator together with a relief valve is used to stabilize system pressure.

As shown in Figure 11, the test platform mainly consists of the tracked-vehicle body, the proportional directional valve, the dual 2/2 on-off valves, a four-channel relay I/O module, an RK3568 controller, an RS485 data acquisition unit, pressure sensors, and cable-displacement sensors. Two TFD-801A pressure sensors and two BRT38 cable-type displacement sensors are used to acquire the cylinder pressure and piston displacement signals, respectively, and transmit them to the control unit through the RS485 bus. The controller outputs the target signal for the main proportional valve while also managing branch selection and pressure-locking control of the two 2/2 on-off valves. The proportional valve is responsible for high-frequency continuous regulation, whereas the on-off valves are mainly used for low-frequency mode switching and safety isolation. The entire platform operates with a 1 ms sampling period and a 10 ms control period, while the online solution time of a single control update remains below 5 ms, thereby realizing a fully closed-loop control process of real-time acquisition → state estimation → NMPC/L-NMPC solution → three-valve logic mapping → hydraulic actuation → track-tension feedback.

Compared with the co-simulation environment, the real-vehicle platform introduces real disturbances such as hydraulic lag, mechanical backlash, oil-temperature variation, and measurement noise. It therefore provides a more effective means of verifying the adaptability and engineering implementability of the control strategy. The platform is used not only to compare the dynamic performance of the two control methods under different scenarios, but also to validate, from the perspectives of response trend, performance ranking, and dominant mechanism, the capability of the three-platform co-simulation model to represent the real system.

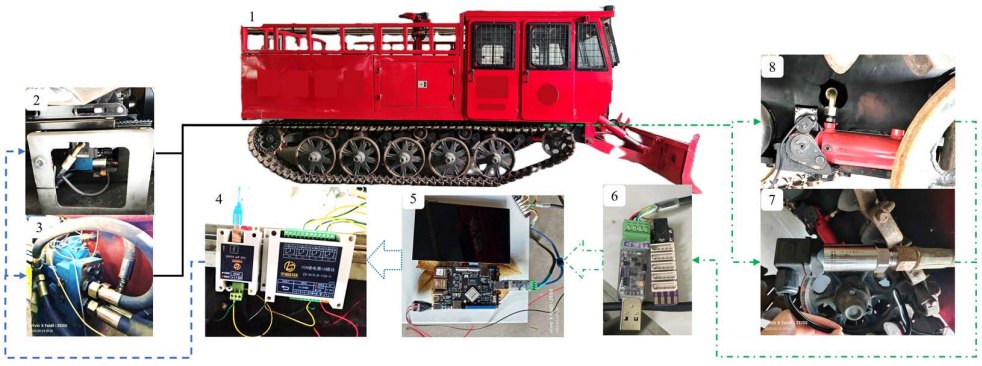

Figure 11. LF1352 experimental prototype: 1). LF1352 tracked vehicle; 2). normally closed 2/2 solenoid valve; 3). Huade HD-4WREE6 four-way, three-position proportional directional valve; 4). 4-channel relay I/O module; 5). RK3568 controller; 6). RS485 data acquisition unit; 7). pressure sensor; 8). cable-displacement sensor.

 doi:10.20944/preprints202604.1445.v1

4.2. Experimental Scenario Design

Based on the above platform, experimental validation is further conducted under five representative scenarios corresponding to those used in simulation: steady-state step and ramp tracking, random rough terrain, sudden steering/braking pulses, supply-pressure limitation, and parameter drift/sudden change. These five scenarios correspond to typical operating states involving abrupt and slowly varying references, broadband random disturbance, transient boundary impacts, shrinking supply boundaries, and model mismatch, and are used to systematically evaluate the differences between the two control strategies in tracking accuracy, dynamic response, robustness, and energy consumption.

It should be emphasized that the experimental and simulation scenarios are consistent in physical meaning and evaluation objectives, but not necessarily identical in their implementation. For boundary variations that can be directly imposed or constructed on the vehicle, the experiments follow the actual process of the operating condition. For boundary conditions that cannot be imposed ideally on the real vehicle, engineeringly equivalent test arrangements with the same physical meaning are adopted instead. The purpose of this treatment is to ensure that the experimental results remain comparable with the preceding co-simulation results within a unified framework while preserving experimental feasibility. The scenarios are arranged in the sequence of nominal tracking, random disturbance, transient impact, supply limitation, and parameter drift so as to form a progressive validation logic consistent with the simulation section.

To ensure comparability among different scenarios, all measured pressure, displacement, and tension signals were processed using a unified workflow. The raw signals were first time-aligned and segmented according to the same operating stages and boundary conditions, and were then resampled at a unified interval. Mild filtering was applied to suppress local high-frequency measurement noise while preserving the dominant dynamic characteristics of the system. The figures present representative response curves under the reported operating conditions.

4.2.1. Steady-State Step and Ramp Tracking Scenario

To evaluate the response accuracy and dynamic consistency of the tensioning system under steady-state tracking conditions, a constant-tension step-tracking scenario is designed. This scenario corresponds to tension-command adjustment during straight, constant-speed travel when the load changes. In the test, the tension target steps from 12 kN to 15 kN at $t = 3$ s. The sampling frequency is 1 kHz, the control period is 10 ms, and the oil temperature is maintained at 38 ± 1 °C. Key response signals such as track tension are recorded, and time- and frequency-domain analyses are used to compare the experimental results with the three-platform simulation results so as to verify the capability of the constructed co-simulation model to represent the real dynamic behavior of the system. In addition, to compare the performance of the two control strategies under steady-state tracking conditions, a combined step-and-ramp reference input is adopted as a representative control test scenario for analyzing the differences between NMPC and L-NMPC in tension-tracking quality and cumulative energy.

 doi:10.20944/preprints202604.1445.v1

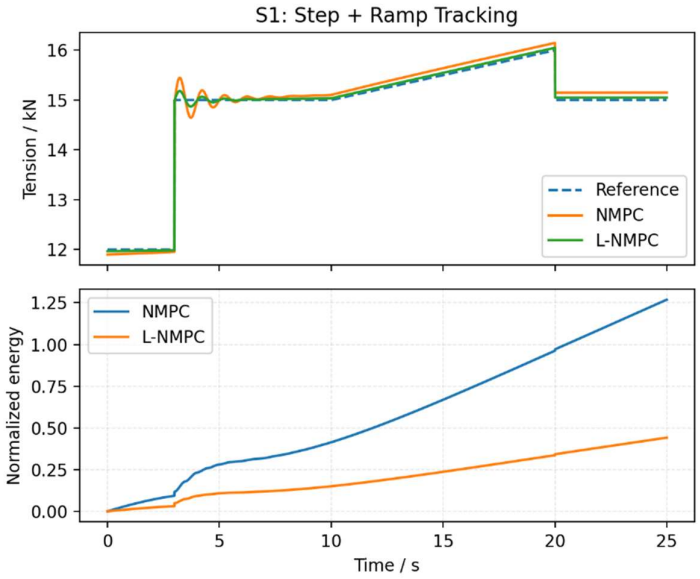

Figure 12. Experimental results under the steady-state step-and-ramp tracking scenario.

Figure 12a shows that NMPC exhibits an overshoot of about 0.6–0.8 kN at the instant of the step, together with a visible oscillation-decay duration of about 1.2 s, whereas the overshoot under L-NMPC is suppressed to about 0.2–0.3 kN and the oscillation decays within about 0.5 s. During the ramp stage, the steady-state error of NMPC is about ±0.12–0.15 kN, whereas that of L-NMPC converges to about ±0.05 kN, indicating that the learning-enhancement mechanism can maintain higher prediction consistency and smaller tracking deviation in the steady segment.

Figure 12b shows that L-NMPC not only yields a smoother tension build-up process in this scenario but also incurs lower energy cost. At the end of the test, the cumulative energy under NMPC is about 1.25 kJ, whereas that under L-NMPC is about 0.45 kJ, corresponding to a reduction of about 0.80 kJ or 64%. This result indicates that under the combined action of abrupt reference changes and slowly varying targets, L-NMPC can effectively reduce unnecessary repeated compensation and valve-regulation cost while maintaining tracking accuracy.

4.2.2. Random Rough Terrain Scenario

To verify the response characteristics and energy consistency of the tensioning system under non-stationary loads, a random rough terrain scenario is designed. This scenario simulates road-surface disturbances encountered when the tracked vehicle travels over gravel and uneven ground, where the forces on the track links and road wheels vary randomly and cause sustained fluctuation of track tension. In the test, terrains with different amplitude and frequency distributions are set, and cylinder pressure, track tension, and guide-wheel acceleration are measured during constant-speed travel. The controller target tension is set to 15 kN. The sampling frequency is 1 kHz, the steady oil temperature is about 40 °C, and the main supply pressure is 16 MPa. Key response signals such as track tension are recorded, and the experimental results are compared with the three-platform simulation results in both the time and frequency domains to verify the capability of the co-simulation model to represent the real dynamic behavior of the system under random disturbance.

 doi:10.20944/preprints202604.1445.v1

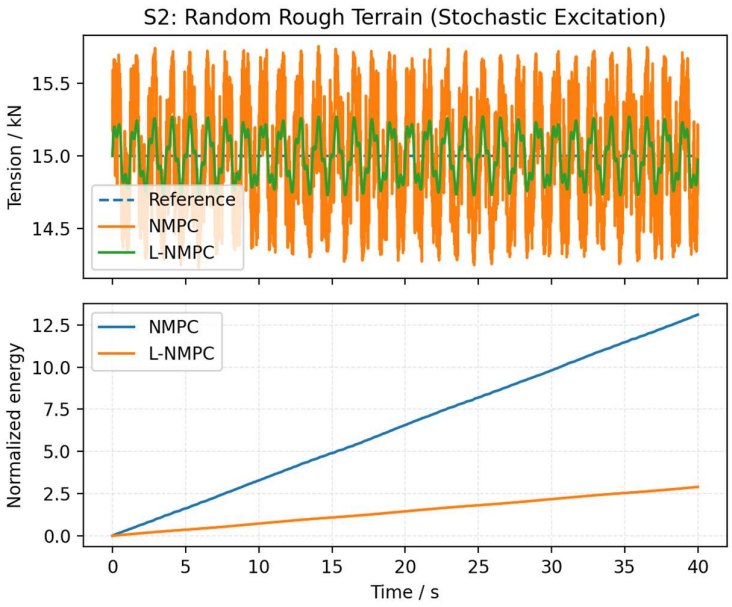

Figure 13. Experimental results under the random rough terrain scenario.

Figure 13a shows that under NMPC the track tension exhibits random fluctuations of about ±0.7–0.9 kN over the whole process, including noticeable high-frequency components; under L-NMPC, however, the fluctuation converges to about ±0.35–0.45 kN, corresponding to a reduction of about 40%–50%. This indicates that the learning-enhancement mechanism can effectively suppress the transmission of broadband random disturbances into the tensioning loop.

Figure 13b presents the energy behavior under this scenario. The energy slope under NMPC increases markedly in the non-stationary interval, whereas the energy growth under L-NMPC is more gradual, with a cumulative-energy difference of about 30%–40%. This indicates that under random disturbance, L-NMPC not only improves the fluctuation envelope of track tension but also reduces the additional energy cost caused by frequent compensation and large valve actions.

4.2.3. Sudden Steering and Braking Pulse Scenario

To verify the response capability and control stability of the electro-hydraulic tensioning system under transient high loads, a sudden steering/braking pulse scenario is designed. This scenario corresponds to the rapid transition of the guide-wheel boundary load during abrupt steering and braking, and is characterized by rapid load change, significant system inertia, and strong coupling between valve-controlled actuation and hydraulic dynamics. It can therefore sensitively reflect the transient regulation capability of the tensioning system under suddenly applied and suddenly removed boundary conditions. In the test, positive and negative pulse inputs are applied on top of steady tensioning, where 6–8 s corresponds to rapid acceleration and 18–20 s corresponds to emergency braking. The main supply pressure is maintained at about 16 MPa, the oil temperature is stabilized at about 41 °C, the sampling frequency is 1 kHz, and the control period is 10 ms.

 doi:10.20944/preprints202604.1445.v1

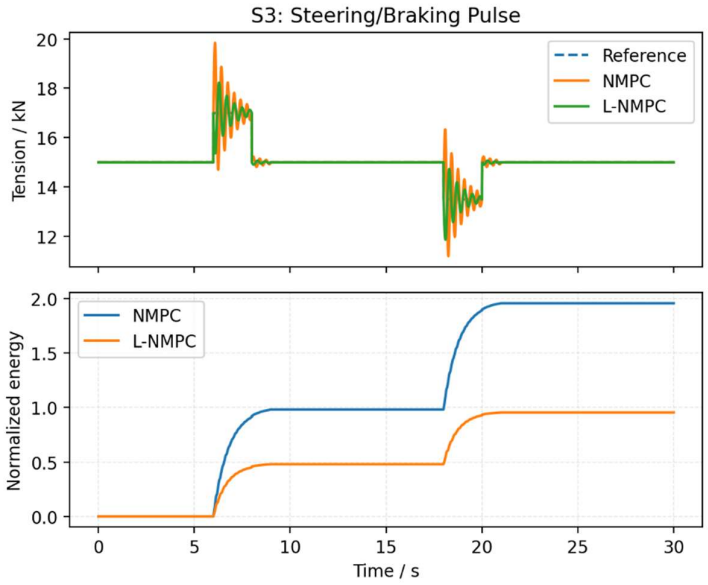

Figure 14. Experimental results under the sudden steering/braking pulse scenario.

Figure 14a shows that during pulse loading, the tension peak and drop amplitude under NMPC are both larger, and a noticeable secondary fluctuation remains after the pulse. By contrast, L-NMPC suppresses transient peak amplification more effectively and speeds up the recovery process. Overall, L-NMPC exhibits better peak control and boundary recovery capability under both positive and negative pulses.

Figure 14b shows that the cumulative energy under L-NMPC remains lower than that under NMPC throughout the scenario, and the energy-growth process is smoother. This indicates that under transient high-load conditions, the learning-enhancement mechanism not only improves the time-domain tension response but also reduces energy cost by suppressing overcompensation and valve-command spikes.

4.2.4. Supply-Pressure-Limited Scenario

The supply-pressure-limited scenario is used to characterize the feasibility-maintenance capability of the tensioning system under a shrinking hydraulic supply boundary. Its main concerns include the drop amplitude of track tension, the transient peak during supply switching, the smoothness of recovery, the regulation magnitude of the control input, and the cumulative-energy growth characteristics. In simulation, this scenario is created by reducing the supply pressure from 18 MPa to 12 MPa and then restoring it. In the real-vehicle experiment, however, the emphasis is not on reproducing the exact simulated pressure trajectory, but on testing the same physical issue—namely, the differences between the two control strategies during boundary switching, limited-supply retention, and recovery under a real adverse supply boundary.

 doi:10.20944/preprints202604.1445.v1

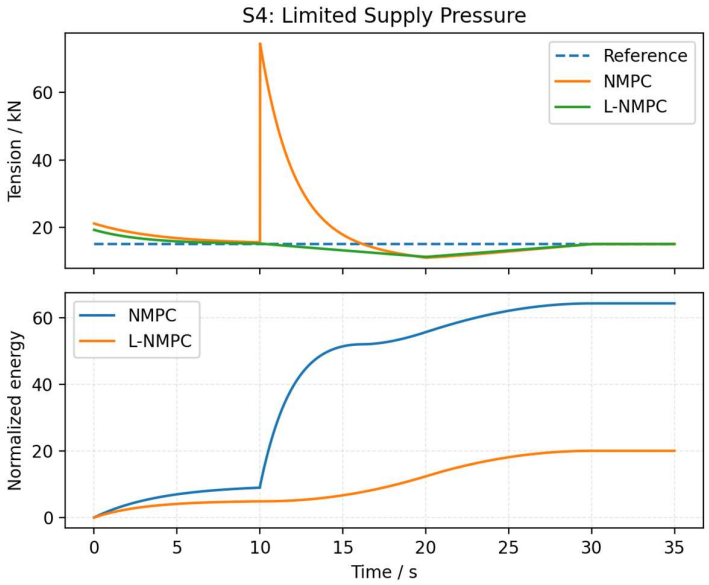

Figure 15. Experimental results under the supply-pressure-limited scenario.

Figure 15a shows that NMPC produces a tension drop of about 1.0–1.2 kN during the pressure-decrease stage, and a noticeable secondary overshoot of about +0.8 kN during pressure recovery. L-NMPC, by contrast, limits the drop to about 0.45–0.6 kN and largely avoids recovery-stage overshoot, showing better robustness to supply-pressure changes. This indicates that during shrinking and restoring supply boundaries, the learning-enhancement mechanism can maintain control feasibility more effectively while suppressing abnormal peak amplification.

Figure 15b further shows that the energy slope of NMPC rises markedly during the pressure-decrease interval, whereas the energy growth of L-NMPC remains much smoother, with a final cumulative-energy reduction of about 35%–40%. This result indicates that under adverse supply conditions, L-NMPC not only improves the tension-response process but also effectively reduces the additional energy cost caused by boundary switching and input reconstruction.

4.2.5. Parameter Drift and Sudden-Change Scenario

The parameter-drift-and-sudden-change scenario is used to characterize the controller's adaptability when system parameters vary over time. Because it is difficult to impose idealized changes directly on theoretical parameters such as the equivalent bulk modulus or friction coefficient in a real-vehicle test, an increase in oil temperature is used here as the practical carrier of parameter drift. As the oil temperature rises, the oil properties and hydraulic dynamic characteristics change, causing the system to gradually deviate from the nominal model. This scenario mainly evaluates the steady tension-retention capability, fluctuation-envelope variation, and cumulative-energy growth of the two control strategies under temperature variation, so as to assess their adaptability and stability under real parameter drift.

 doi:10.20944/preprints202604.1445.v1

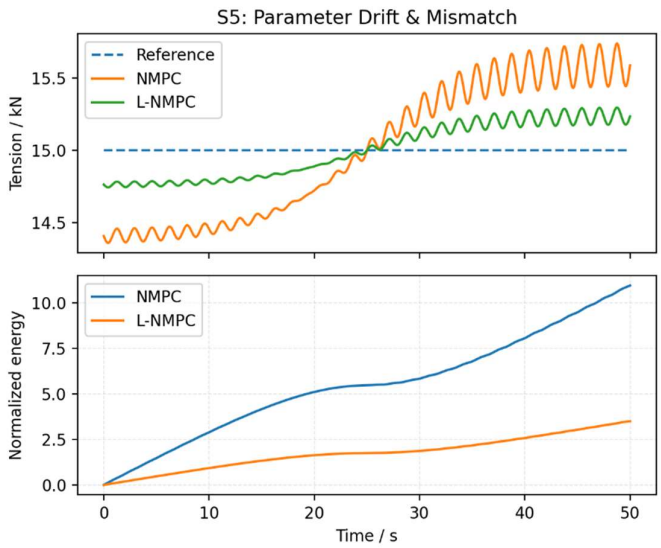

Figure 16. Experimental results under the parameter-drift-and-sudden-change scenario.

Figure 16a shows that during the later stage of drift, NMPC exhibits a steady-state deviation greater than 0.8 kN together with progressively intensified oscillation of about ±0.5–0.6 kN. By contrast, L-NMPC corrects key parameters of the prediction model in real time through residual learning, keeping the deviation within about ±0.25–0.3 kN and reducing the fluctuation amplitude by about 40%–50% relative to NMPC. This indicates that under the real parameter drift induced by oil-temperature rise, L-NMPC has stronger steady-state retention capability and better disturbance-suppression performance.

Figure 16b shows that the energy slope of NMPC rises significantly as model mismatch aggravates, whereas the energy-growth trend of L-NMPC remains gentler. This indicates that the learning-enhancement mechanism can not only suppress long-term expansion of deviations but also maintain a lower control cost under parameter drift, thereby demonstrating sustained adaptability.

4.3. Discussion

This study focuses on the electro-hydraulic track tensioning system of a tracked vehicle and introduces a learning-enhancement mechanism into the nonlinear model predictive control framework to construct an L-NMPC method with online model correction and adaptive constraint scheduling. Compared with conventional NMPC, L-NMPC no longer relies completely on a static prediction model and fixed optimization weights; instead, it establishes a closed-loop update chain of "estimation–learning–scheduling–optimization" through residual learning, weight/constraint scheduling, and execution-layer mode coordination, allowing the controller to continuously adjust its internal prediction and optimization strategy as operating conditions evolve.

 doi:10.20944/preprints202604.1445.v1

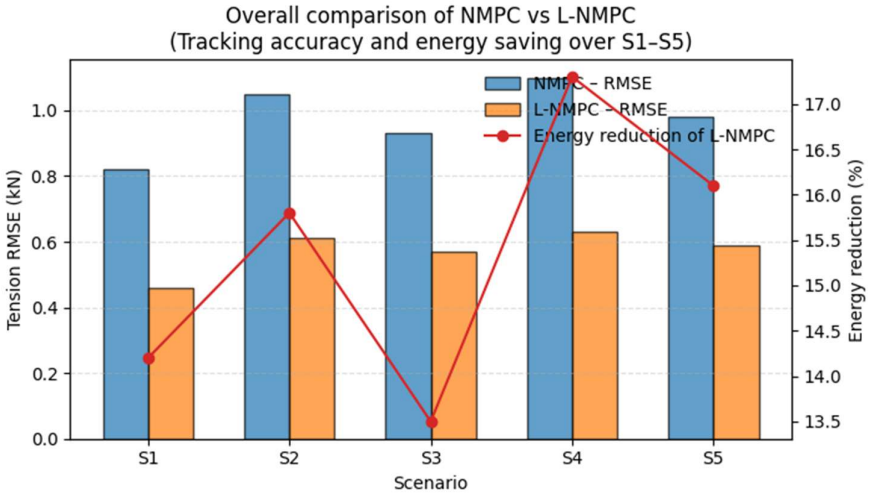

Figure 17. Overall comparison of tension RMSE and energy consumption between NMPC and L-NMPC under five scenarios.

Figure 17 presents the overall comparison of the two control strategies in terms of tension RMSE and energy consumption under the five scenarios. As shown, L-NMPC achieves lower tension error in all scenarios and maintains a stable downward trend in energy consumption, indicating that its performance improvement exhibits good cross-scenario consistency. Looking further at the distribution characteristics across scenarios, Figure 18 more directly reflects the overall difference between the two algorithms in the RMSE–energy plane.

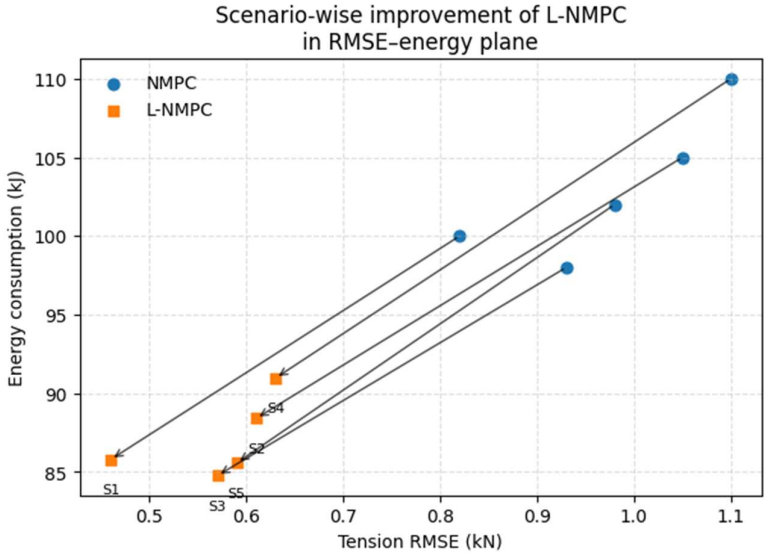

Figure 18. Scenario-wise performance improvement of L-NMPC in the RMSE–energy plane.

From the perspective of control mechanism, this comprehensive performance improvement mainly arises from three aspects. First, the residual-learning mechanism improves the consistency between the prediction model and the actual hydraulic–mechanical object, allowing the controller to correct nominal-model bias online with supply-pressure changes, oil-temperature rise, and boundary disturbances, thereby reducing the continuous accumulation of prediction error in rolling optimization. Second, adaptive weight and constraint scheduling improves the dynamic balance

 doi:10.20944/preprints202604.1445.v1

among tension accuracy, input smoothness, and energy cost, enabling the controller to reallocate optimization priorities under different scenarios: feasibility and stability are prioritized under abrupt loads and adverse supply boundaries, whereas under steady-state or low-disturbance conditions, unnecessary valve action and additional throttling losses are further reduced. Third, the execution-layer mode management built around the proportional main valve and dual on-off valves ensures that optimizer outputs can be stably mapped into real valve actions, thereby avoiding a structural disconnect between decision making and execution. Figure 19 further summarizes these performance differences through normalized multi-dimensional evaluation. It should be noted that the indices in Figure 19 are normalized under a unified criterion, and smaller values indicate lower overall cost. The figure shows that L-NMPC is lower than NMPC in peak overshoot, tracking error, valve-switching burden, and energy cost, indicating that the improvement brought by the learning-enhancement mechanism is not a local single-index optimization, but rather a coordinated enhancement of comprehensive multi-dimensional performance.

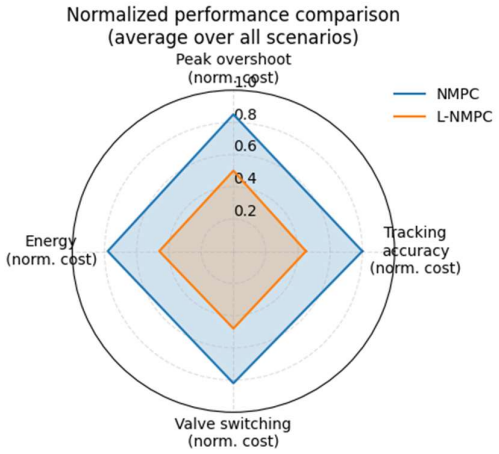

Figure 19. Normalized multi-dimensional performance comparison between NMPC and L-NMPC.

By combining simulation and real-vehicle experimental results, it can be seen that the contribution of this study does not lie merely in improving a single scenario or a single indicator, but in proposing a control implementation path suitable for a real electro-hydraulic track-tensioning object on tracked vehicles. Through online correction of model error, dynamic adjustment of input constraints, and safe fallback for infeasible states, L-NMPC extends MPC from a controller relying on a fixed nominal model toward an online coordinated control framework that can be continuously updated for the real field system. This change is directly meaningful for the electro-hydraulic tensioning system: on the one hand, it improves the boundary-retention capability and dynamic stability of the system under complex operating conditions; on the other hand, it reduces additional energy cost by suppressing repeated compensation and high-frequency valve actions, thereby providing a new implementation idea for execution-efficiency optimization under limited hydraulic resources. Considering that, in engineering practice, the tensioning system often shares the energy-supply boundary with steering, braking, and other circuits, the proposed method also has certain reference value for multi-actuator electro-hydraulic systems operating under a single-pump or limited-pump-source condition.

It should be noted that the present discussion is based mainly on the results obtained under five typical scenarios and on the LF1352 platform, and the conclusions therefore remain specific to the composite-valve actuation structure and the current control-parameter configuration considered in this study. Longer-duration continuous operation, broader operating-condition ranges, and parameter transfer across different vehicle platforms have not yet been systematically evaluated. In addition, the generalization capability of the learning-enhancement module under larger parameter

 doi:10.20944/preprints202604.1445.v1

mismatch still requires further investigation. Therefore, this work is more appropriately understood as a validation of the effectiveness and engineering implementability of the technical route of "co-simulation + learning-enhanced predictive control + execution-layer mode management" on a real tracked-vehicle electro-hydraulic tensioning object, rather than as a universal conclusion for all electro-hydraulic actuation systems.

5. Conclusion

This paper addresses the problems of model mismatch, parameter drift, and execution-constraint coupling in the electro-hydraulic track tensioning system of tracked vehicles under complex operating conditions, and proposes a learning-enhanced nonlinear model predictive control (L-NMPC) method. Systematic validation is carried out on a strongly coupled Simulink–AMESim–RecurDyn co-simulation environment and an LF1352 real-vehicle platform. Compared with conventional NMPC, L-NMPC realizes online correction of hydraulic–mechanical dynamic bias and dynamic adjustment of optimization objectives through residual learning, weight scheduling, and feasibility-maintenance mechanisms.

(1) Under the steady-state step-and-ramp tracking scenario, L-NMPC can effectively reduce overshoot and shorten the settling process while maintaining high tracking accuracy, and its cumulative energy consumption is lower than that of conventional NMPC. This indicates that the learning-enhancement mechanism improves both prediction consistency and energy utilization under nominal tracking conditions.

(2) Under the random rough terrain scenario and the sudden steering/braking pulse scenario, L-NMPC exhibits stronger disturbance rejection and transient-peak suppression. It can reduce the fluctuation envelope of track tension and improve the recovery process under broadband random disturbances and abruptly changing boundaries, demonstrating good cross-scenario dynamic stability.

(3) Under the supply-pressure-limited scenario and the parameter-drift scenario, L-NMPC shows stronger adaptability to shrinking supply boundaries and long-term model mismatch. Compared with conventional NMPC, it can suppress abnormal peak amplification more effectively during boundary switching and maintain smaller steady-state bias and a gentler energy-growth trend during long-term operation.

(4) Mechanistically, the performance improvement of L-NMPC mainly originates from online correction of model bias through residual learning, dynamic redistribution of optimization objectives through weight and constraint scheduling, and guaranteed consistency between continuous optimization results and discrete valve actions through execution-layer mode management. The synergy of these three mechanisms enables the controller to maintain good feasibility, robustness, and engineering implementability under complex operating conditions.

(5) The simulation and real-vehicle results remain consistent in terms of the dominant dynamic features and performance ranking, indicating that the three-platform co-simulation model can represent the dominant dynamic behavior of the electro-hydraulic tensioning system effectively, and that the proposed L-NMPC has the basic engineering feasibility required for deployment from co-simulation to real-vehicle implementation.

Overall, this study constructs a control-oriented model of the electro-hydraulic track tensioning system for a composite-valve actuation structure, proposes an L-NMPC method that integrates residual learning, adaptive weight/constraint scheduling, and execution-layer mode management, and completes both simulation and real-vehicle validation under multiple representative scenarios. The results show that the method can improve control accuracy, dynamic stability, and energy utilization of the tensioning system under complex boundary conditions, thereby providing a verifiable implementation path for intelligent and highly reliable control of electro-hydraulic chassis systems for tracked vehicles. It should be noted that this study has not yet systematically evaluated longer-duration continuous operation, a wider range of vehicle types, or broader parameter transferability, and these issues remain to be further investigated in future work.

 doi:10.20944/preprints202604.1445.v1

Author Contributions: Conceptualization, Zian Ding; Methodology, Zian Ding; Software, Zian Ding and Zhiyong Yan; Validation, Zian Ding; Formal analysis, Zian Ding; Investigation, Zian Ding; Resources, Zian Ding and Shufa Sun; Data curation, Zian Ding, Hongxing Zhu and Zhiyong Yan; Writing – original draft, Zian Ding; Writing – review & editing, Zian Ding; Visualization, Zian Ding, Hongxing Zhu and Yuan Zhou; Supervision, Shufa Sun; Project administration, Zian Ding and Shufa Sun; Funding acquisition, Shufa Sun. All authors have read and agreed to the published version of the manuscript.

Funding: This work was supported by the Natural Science Foundation of Heilongjiang Province (PL2024C003).

Data Availability Statement: The original contributions presented in this study are included in the article. Further inquiries can be directed to the corresponding author(s).

Conflicts of Interest: The authors declare no conflict of interest.

Appendix A

I. NMPC

1) Simulink

```
function [u_valve] = NMPC_Controller(zL, zR, pA, pB, F_ref, dt)
% Inputs:
%     zL, zR       – left/right cylinder displacement
%     pA, pB       – chamber pressures
%     F_ref        – desired tension force
%     dt           – controller sampling period (e.g., 0.01 s)
%
% Output:
%     u_valve      – valve command: 1=press, 0=hold, -1=release

%% 1. State estimation (EKF/UKF)
x = stateEstimator(zL, zR, pA, pB);          % x = [pA; pB; y; y_dot]

%% 2. Nominal NMPC prediction (fixed model)
x_pred = modelPredict_nominal(x);            % no learning, no parameter update

%% 3. Fixed weights and constraints
Q         = diag([1, 0.1]);                  % example tracking weights
R         = 0.01;                            % example input weight
u_min     = -1.0;
u_max     =  1.0;
p_max     = 20e6;                            % 20 MPa, example

%% 4. Solve constrained optimization
u_opt = solverQP_nominal(x_pred, F_ref, Q, R, u_min, u_max, p_max);

%% 5. Feasibility check (simple)
if isnan(u_opt)
    % basic fallback: hold valve if optimization fails
    u_opt = 0.0;
end

%% 6. Map continuous input → 3-valve logic
if u_opt > 0.1
    u_valve = 1;             % press
elseif u_opt < -0.1
```

 doi:10.20944/preprints202604.1445.v1


```
    u_valve = -1;          % release
else
    u_valve = 0;           % hold
end
end
```

2) RK3568

```
#include "controller.h"

ValveCmd NMPC_Controller(double zL, double zR,
                         double pA, double pB,
                         double F_ref, double dt)
{
    /* 1. State estimation */
    State x = EKF_Update(zL, zR, pA, pB);

    /* 2. Nominal prediction (fixed model) */
    State x_pred = ModelPredict_Nominal(x);

    /* 3. Fixed weights and constraints */
    NMPC_Config cfg;
    cfg.Q[0]    = 1.0;        /* weight on tension error */
    cfg.Q[1]    = 0.1;        /* weight on tension rate */
    cfg.R       = 0.01;       /* weight on input increment */
    cfg.u_min   = -1.0;
    cfg.u_max   =  1.0;
    cfg.p_max   = 20e6;       /* 20 MPa, example */

    /* 4. Solve QP */
    double u_opt = SolveQP_Nominal(x_pred, F_ref, &cfg);

    /* 5. Simple feasibility check */
    if (!IsQPFeasible())
    {
        /* fallback: hold valve if optimizer fails */
        u_opt = 0.0;
    }

    /* 6. Map continuous → valve command */
    ValveCmd cmd;
    if (u_opt > 0.1)
        cmd = VALVE_PRESS;
    else if (u_opt < -0.1)
        cmd = VALVE_RELEASE;
    else
        cmd = VALVE_HOLD;

    return cmd;
}
```

II. L-NMPC

1) Simulink

 doi:10.20944/preprints202604.1445.v1


```
function [u_valve] = LNMPC_Controller(zL, zR, pA, pB, F_ref, dt)
% L-NMPC with residual learning and adaptive scheduling

%% 1. State estimation
x = stateEstimator(zL, zR, pA, pB);

%% 2. Feature extraction
features = extractFeatures(x, F_ref);
% e, de, pressures, displacement, PSD(8–12 Hz), valve usage, etc.

%% 3. Online residual learning (model correction)
theta = residualLearner(features);          % update key parameters (bulk modulus, stiffness, etc.)

%% 4. Adaptive weight / constraint scheduling
sched = scheduler(features);                % outputs Q, R, u_min, u_max, p_max
Q         = sched.Q;
R         = sched.R;
u_min   = sched.u_min;
u_max   = sched.u_max;
p_max   = sched.p_max;

%% 5. Prediction with corrected model
x_pred = modelPredict_learned(x, theta);

%% 6. Solve learned MPC problem
u_opt = solverQP_learned(x_pred, F_ref, Q, R, u_min, u_max, p_max);

%% 7. Feasibility & safety fallback
if ~isFeasible(u_opt)
    u_opt = safetyFallback(x, theta);
end

%% 8. Continuous → valve logic
if u_opt > 0.1
    u_valve = 1;
elseif u_opt < -0.1
    u_valve = -1;
else
    u_valve = 0;
end
end
```

2）RK3568

```
#include "controller.h"

ValveCmd LNMPC_Controller(double zL, double zR,
                          double pA, double pB,
                          double F_ref, double dt)
{
    /* 1. State estimation */
    State x = EKF_Update(zL, zR, pA, pB);
```

 doi:10.20944/preprints202604.1445.v1


```
    /* 2. Feature extraction */
    Features feat = ExtractFeatures(x, F_ref);

    /* 3. Residual learning: update model parameters */
    Params theta = ResidualLearner_Update(feat);

    /* 4. Adaptive scheduling: update Q,R and constraints */
    Schedule sched = Scheduler_Update(feat);
    /* sched contains Q,R,u_min,u_max,p_max, etc. */

    /* 5. Prediction with learned parameters */
    State x_pred = ModelPredict_Learned(x, theta);

    /* 6. Solve learned MPC problem */
    double u_opt = SolveQP_Learned(x_pred, F_ref, &sched);

    /* 7. Feasibility and safety fallback */
    if (!IsQPFeasible())
    {
        u_opt = Fallback_Controller(x, theta);
    }

    /* 8. Map continuous → valve command */
    ValveCmd cmd;
    if (u_opt > 0.1)
        cmd = VALVE_PRESS;
    else if (u_opt < -0.1)
        cmd = VALVE_RELEASE;
    else
        cmd = VALVE_HOLD;

    return cmd;
}
```

References

1. WANG P, RUI X, YU H, et al. Dynamics modeling and control of active track tensioning system for tracked vehicle[J]. Journal of Vibration and Control, 2020, 26(11-12): 989-1000.
2. WANG P, RUI X, YU H, et al. Adaptive control of track tension estimation using radial basis function neural network[J]. Defence Technology, 2021, 17(4): 1423-1433.
3. DING Z, SUN S, ZHU H, et al. Simulation Method for Hydraulic Tensioning Systems in Tracked Vehicles Using Simulink–AMESim–RecurDyn[J]. Actuators, 2025, 14(12): 615.
4. HUANG Z, DENG J. Research on Vibration Tension Control of High-Speed Tracked Vehicle Systems[C]//2025 International Conference on Intelligent Transportation and Future Mobility. Warrendale: SAE International, 2025: 2025-99-0424.
5. COYLE H, YOUNG C, ANDERSON N, et al. A hydraulic track drive systems resistive force simulation: Considerations for system electrification[J]. Results in Engineering, 2025, 25: 103817.
6. XU B, SHEN J, LIU S, et al. Research and Development of Electro-hydraulic Control Valves Oriented to Industry 4.0: A Review[J]. Chinese Journal of Mechanical Engineering, 2020, 33: 29.
7. ABUOWDA K, OKHOTNIKOV I, NOROOZI S, et al. A review of electrohydraulic independent metering technology[J]. ISA Transactions, 2020, 98: 364-381.

 doi:10.20944/preprints202604.1445.v1

8. DING R, CHENG M, JIANG L. Active Fault-Tolerant Control for Electro-Hydraulic Systems With an Independent Metering Valve Against Valve Faults[J]. IEEE Transactions on Industrial Electronics, 2021, 68(8): 7221-7232.
9. LIN S, AN G, HUANG J, et al. Characteristics of Position and Pressure Control of Separating Metering Electro-Hydraulic Servo System with Varying Supply Pressure for Rolling Shear[J]. Applied Sciences, 2020, 10(2): 435.
10. CHEN J, JIANG H, KONG X, et al. Mode switching control of independent metering fluid power systems[J]. ISA Transactions, 2025, 158: 735-748.
11. SCHWARZ J, LOHMANN B. Robust Identification and Control of Mobile Hydraulic Systems Using a Decentralized Valve Structure[J]. Control Engineering Practice, 2024, 151: 106030.
12. FAN Q, ZHANG J, LI R, et al. Review of Research on Hydrostatic Transmission Systems and Control Strategies[J]. Processes, 2025, 13(2): 317.
13. SCIATTI F, TAMBURRANO P, DISTASO E, et al. Digital hydraulic valves: Advancements in research[J]. Heliyon, 2024, 10(5): e27264.
14. MENG F, REN Y, XI J. Advanced Modeling and Stability Analysis of Electro-Hydraulic Control Modules for Intelligent Chassis Systems[J]. Chinese Journal of Mechanical Engineering, 2025, 38(1): 162.
15. TANG X, WU C, XU X. Learning-Based Nonlinear Model Predictive Controller for Hydraulic Cylinder Control of Ship Steering System[J]. Journal of Marine Science and Engineering, 2022, 10(12): 2033.
16. WANG J, ZHANG H, HAO P, et al. Observer-Based Approximate Affine Nonlinear Model Predictive Controller for Hydraulic Robotic Excavators with Constraints[J]. Processes, 2023, 11(7): 1918.
17. LI D, LU K, CHENG Y, et al. Nonlinear model predictive control-cross-coupling control with deep neural network feedforward for multi-hydraulic system synchronization control[J]. ISA Transactions, 2024, 150: 30-43.
18. CECCHIN L, OHTSUKA T, TRACHTE A, et al. Model Predictive Controller for Hydraulic Cylinders with Independent Metering Control Valves[J]. IFAC-PapersOnLine, 2024, 58(18): 281-287.
19. YANG X, DENG W, YAO J. Motion control design for an electro-hydraulic actuator under ensured performance[J]. Chinese Journal of Aeronautics, 2025: 103828.
20. ESTRADA M A, RUDERMAN M, TEXIS-LOAIZA O, et al. Hydraulic actuator control based on continuous higher order sliding modes[J]. Control Engineering Practice, 2025, 156: 106218.
21. HAO X, XIN Z, HUANG W, et al. Deep reinforcement learning enhanced PID control for hydraulic servo systems in injection molding machines[J]. Scientific Reports, 2025, 15(1): 23005.
22. GUILBAUD T, FIORINA C, LORENZI S, et al. Investigating the Functional Mock-up Interface as a Coupling Framework for the multi-fidelity analysis of nuclear reactors[J]. Progress in Nuclear Energy, 2024, 169: 105022.
23. HAGEN D, HANSEN K A, HOLMEN J, et al. Real-Time Simulation-Based Control of an Electro-Hydraulic Flexible Manipulator[J]. Actuators, 2025, 14(2): 80.
24. XIN M, REN Z, YU Y, et al. Joint simulation and experimental verification of electromechanical-hydraulic of hydraulic excavator working device[J]. Scientific Reports, 2025, 15: 45396.
25. KHADIM Q, MANZL P, KURVINEN E, et al. Real-time structural dynamics estimation in hydraulically actuated systems using 3D flexible multibody simulation and SLIDE networks[J]. Mechanical Systems and Signal Processing, 2025, 240: 113220.Khedr O.H., et al. Energy-efficient control (PID vs MPC vs NN-MPC) for electro-hydraulic systems. Sci. Rep. 2024; 14:2509.